Magnetic Resonance Imaging of the Heart and Vasculature at 3 Tesla:

Novel Strategies for the Diagnosis and Risk Stratification of Cardiovascular Disease

APPROVED BY SUPERVISORY COMMITTEE

Committee Chairperson's Name _____

Dr. Ronald M. Peshock

Committee Member's Name _____

Dr. Alice Y. Chang

Committee Member's Name _____

Dr. Michael McPhaul

Magnetic Resonance Imaging of the Heart and Vasculature at 3 Tesla:

Novel Strategies for the Diagnosis and Risk Stratification of Cardiovascular Disease

by

Christopher D. Maroules, B.S.

DISSERTATION

Presented to the Faculty of the Medical School

The University of Texas Southwestern Medical Center at Dallas

In Partial Fulfillment of the Requirements

For the Degree of

DOCTOR OF MEDICINE WITH DISTINCTION IN RESEARCH

The University of Texas Southwestern Medical Center at Dallas

Dallas, Texas

February 25, 2009

TABLE OF CONTENTS

ABSTRACT

Magnetic Resonance Imaging of the Heart and Vasculature at 3 Tesla:

Novel Strategies for the Diagnosis and Risk Stratification of Cardiovascular Disease

CHRISTOPHER D. MAROULES

The University of Texas Southwestern Medical Center at Dallas

Supervising Professor: Dr. Ronald M. Peshock

Purpose: (1) To study the effects of field strength and parallel imaging on image contrast and the interstudy reproducibility of right and left ventricular (RV and LV) measurements using steady-state free precession (SSFP) cardiac magnetic resonance; (2) to explore the impact of 3T parallel imaging techniques on the assessment and reproducibility of black-blood aortic atherosclerosis imaging; and (3) to evaluate the feasibility of coronary sinus flow imaging by 3T spiral velocity-encoded cine (VEC) MR imaging in overweight women with risk factors for cardiovascular disease

Materials and Methods: To evaluate cardiac measurements and aortic atherosclerosis by cardiac magnetic resonance, thirty-two subjects (20 normal, 12 cardiac patients) underwent SSFP cine short-axis imaging and black-blood abdominal aortic imaging: two studies at 1.5T, one study at 3T, and another study at 3T with parallel imaging (SENSE). Contrast-to-noise ratios (CNR) were compared between techniques.

To evaluate the feasibility of coronary sinus flow MR imaging, ten women (age 38 years ± 10) with a mean BMI of 33 kg/m^2 ± 8 were studied. Coronary sinus flow was measured at baseline and in response to cold pressor stress. Changes in right coronary artery flow were also measured before and after stress using VEC MRI.

Results: *Cardiac MRI:* 3T SENSE imaging reduced cardiac imaging time from 8 ± 2 min to 3 ± 1 min (P<0.001). A significant gain in LV CNR was detected between 1.5T and 3T with SENSE (43.8 ± 6.5 vs 48.4 ± 7.4, P=0.01), but no significant gain was detected in RV CNR. The reproducibility of LV and RV measurements between two 1.5T studies was not significantly different from the reproducibility between a 1.5T study and a 3T study with SENSE.

Aortic MRI: Image quality scores were comparable between 1.5-T and 3-T with SENSE (4.0 ± 0.6 vs 4.2 ± 0.6, P = 0.21). Bland-Altman reproducibility for MWT was -0.03 mm ± 0.15 (1.5-T vs 1.5-T) and -0.01 mm ± 0.18 (1.5-T vs 3-T with SENSE), P = 0.83. Detection of the presence of absence of plaque was comparable.

Coronary Sinus Flow Imaging: A significant 24% increase in coronary sinus volume flow was observed from baseline to peak cold pressor stress (141 ± 34 ml/min vs. 184 ± 42 ml/min, p = 0.02). Similar increases in RCA flow velocity were observed (15.3 ± 5 cm/sec vs. 23.2 ± 7 cm/sec, P < 0.01).

Conclusions: (1) SSFP cardiac MR imaging and black-blood aortic MR imaging are reproducible techniques. (2) Parallel imaging at 3T permits shorter scan time compared to conventional 1.5-T imaging with comparable measurements of cardiac structure and function, as well as aortic atherosclerosis. (3) Coronary sinus spiral velocity-encoded MRI at 3T is a feasible technique for measuring changes in coronary flow in asymptomatic overweight and obese women with risk factors for cardiovascular disease.

PRIOR PUBLICATIONS & PRESENTATIONS

PUBLICATIONS

Maroules, C.D., Chang, A.Y., Dimitrov, I., Kontak, A., Hadav, Y., Peshock, R.M. (2009) Coronary Sinus Flow Reserve in Response to Cold Pressor Stress using Velocity-Encoded Cine (VEC) Spiral 3T MRI: A Feasibility Study in At-Risk Women. *Journal of Cardiovascular Magnetic Resonance*. Submitted for Review.

Maroules, C.D., Linz, N.A., Boswell, G.E. (2008) Evaluation of Recurrent Takotsubo's Cardiomyopathy by Dual-Source 64-Slice Computed Tomography with MRI Correlation: A Case Report. *Journal of Cardiovascular Computed Tomography*. Provisional Acceptance Pending Revisions.

Chang, A. Y., Kotys, M., Dimitrov, I., Kontak, A., Yadav, H., **Maroules, C.D.**, Tillery, T., Peshock, R.M. (2009). Coronary Artery Flow Velocity Reserve During the Cold Pressor Test in Overweight, Healthy Women Using Spiral Imaging at 3T. *Journal of Cardiovascular Magnetic Resonance* 11(1), 43-44.

Maroules, C.D., McColl, R., Khera, A., Peshock, R.M. (2008) Assessment of Aortic Atherosclerosis MR Imaging: Impact of 3-Tesla Field Strength and Parallel Imaging. *Investigational Radiology*. September; 43(9):656-662.

Maroules, C.D., McColl, R., Khera, A., Peshock, R.M. (2008) Interstudy Reproducibility of SSFP Cine Magnetic Resonance: Impact of Magnetic Field Strength and Parallel Imaging. *Journal of Magnetic Resonance Imaging*; 27(5):1139-45.

Casper, D.M, Blackburn, J.R., **Maroules, C.D**., et al. (2002) Conformational Studies of N^3-Substituted [1,3,4]-oxadiazin-2-ones. *Journal of Organic Chemistry* 67(25), 8871-76.

Hitchcock, S.R., Nora, G.P., **Maroules, C.D**., et al. (2001) X-ray Crystallographic and 13C NMR Studies of 3,4,5,6-Tetrahydro-2H-1,3,4-oxazolidin-2-ones Derived from Ephedrine and Pseudoephedrine. *Tetrahedron*. 57, 9789-98.

PRESENTATIONS

Maroules, C.D. Chang, A.Y., Dimitrov, I., Kontak, A., Peshock, R.M. (2009) Coronary Sinus Flow Imaging in Response to Cold Pressor Stress in Healthy Women Using Velocity-Encoded Cine (VEC) Spiral 3T MRI. Presented at the Annual Symposium of the Society of Magnetic Resonance Imaging. Orlando, FL.

Maroules, C.D., Yadav, H., Peshock, R.M., Chang, A.Y. (2009) Measurement of Impaired Coronary Vascular Reactivity Using 3T MRI in Asymptomatic Women with Type 2 Diabetes. Presented at the Southern Regional Meeting of the American Federation for Medical Research. New Orleans, LA.

Maroules, C. D. and R. Peshock (2007). Accelerated MR Imaging of the Heart and Abdominal Aorta at 1.5 and 3.0 Tesla. Presented at the Annual Doris Duke Clinical Research Symposium. Harvard Medical School. Boston, MA.

Maroules, C. D. and G. L. Hortin (2003). Macromolecular Chromogenic Substrates for Measuring Proteinase Activity In Vivo. Presented at the National Institutes of Health Biomedical Research Symposium, Bethesda, MD.

Maroules, C. D. and S. R. Hitchcock (2002). Synthesis and Asymmetric Application of 3,4,5,6-Tetrahydro-2H-1,3,4-oxazolidin-2-ones Derived from (1R,2S)-Ephedrine. Presented at the 222nd National Conference of the American Chemical Society. Chicago, IL.

List of ABBREVIATIONS

BTFE	Balanced turbo field echo
CMR	Cardiovascular magnetic resonance
CPT	Cold pressor test
CS	Coronary sinus
EDV	End-diastolic volume
EF	Ejection fraction
ESV	End-systolic volume
LVM	Left ventricular mass
PC	Phase contrast
RCA	Right coronary artery
RVM	Right ventricular mass
SSFP	Steady state free precession
SV	Stroke volume
VEC	Velocity-encoded cine

CHAPTER ONE

SSFP Cine Magnetic Resonance Imaging at 3 Tesla: Impact of Magnetic Field Strength and Parallel Imaging

Introduction

Cine steady-state free precession (SSFP) cardiovascular magnetic resonance (CMR) at 1.5T is considered the gold standard for characterizing cardiac anatomy, myocardial mass, and ventricular function for both the left and right ventricles (LV and RV).(1-3) Although several studies have demonstrated the superior reproducibility of CMR compared to echocardiography(4) and nuclear techniques(5), interstudy variability of the SSFP technique has not been extensively investigated.

Recently, clinical magnetic resonance at 3T has become widely available which increases the signal obtained during imaging (6). Parallel imaging algorithms such as sensitivity encoding (SENSE) can be used in this setting to decrease scan time (7). Shorter scan times could potentially improve patient compliance and expedite CMR imaging studies.

As 3T CMR becomes established in clinical practice, there will be an increasing need to compare new patient studies with prior 1.5T exams. Recognizing differences in image quality between the two methods will be important for accurate study interpretation (6,8). Furthermore, measurement variability between accelerated 3T studies and conventional 1.5T studies must be quantified to ensure differences between two studies obtained at different field strengths are valid.

In the present study we asked the following questions: first, how does accelerated 3T CMR affect signal and contrast of the LV and RV compared with standard 1.5T SSFP methods; and second, how does interstudy reproducibility between an accelerated 3T study and a conventional 1.5T study compare to the interstudy reproducibility between two 1.5T studies?

Materials and Methods

Study Participants

Twenty healthy volunteers (12 female and 8 male, mean age 51 ± 14 years) and twelve patients with impaired LV function (3 female and 9 male, mean age 52 ± 10 years) were recruited for this study. Of the patients with impaired LV function, 10 had angiographic evidence of coronary artery disease (CAD) and 2 were diagnosed with dilated cardiomyopathy. Sample population demographics are presented (Table 1)**.** All subjects were in sinus rhythm throughout the study. Subjects were excluded from the study if they had any contraindication to CMR. The study was approved by the local Institutional Review Board and written informed consent was obtained from all subjects.

CMR Protocol

Images were obtained using a 3T system (Achieva; Philips Medical Systems, Best, The Netherlands) and a 1.5T system (Achieva; Philips Medical Systems, Best, The Netherlands) which were operated by different technologists. All subjects underwent four cine SSFP imaging sessions on the same day: Study A consisted of cine imaging at 1.5T without SENSE. Study B consisted of cine imaging at 3T without SENSE. Study C consisted of accelerated imaging at 3T using SENSE, with an acceleration factor of $R = 3$. Study D consisted of another non-accelerated imaging study at 1.5T (identical to Study A). Subjects were randomized to one of

three study sequences to minimize confounding by a training effect: Study A-B-C-D, Study B-C-A-D, or Study A-D-B-C. Between each study, subjects were ambulated between 15-30 minutes before being repositioned on the MR bed. Scout films from the initial CMR study were used as guides for slice co-registration in all subsequent studies.

Images were obtained in all studies using four-element surface array coils (2 anterior and 2 posterior) placed over the subject's chest. Scout images were used to localize the short axis orientation of the heart with selection of the optimal frequency offset. Each study included a SSFP cine series of 10-13 short axis slices spanning the cardiac apex through the ventricular base with temporal resolution $\leq$ 40 milliseconds. Slices were acquired during 15-20 second end-expiratory breath-holds using retrospective ECG-gating. Patients were trained to perform end-expiratory breath holds before the first study. Typical parameters included: field of view (FOV) = 360 mm x 293 mm, matrix size = 256 x 224 (in-plane resolution of 1.4 mm $\times$ 1.3 mm), TR = 4.2 msec, TE = 2.1 msec, slice thickness = 6 mm, slice gap = 4 mm, flip angle = 70^{o} at 1.5T and 30^{o} at 3T. All images were acquired using volume shimming at both 1.5 and 3 T. All imaging was performed within standard SAR limits.

Signal and Contrast Assessment

In each study, signal intensity (SI) measurements were determined by averaging end-diastolic and end-systolic signals from identical circular regions of interest (ROI) in the myocardium, LV blood pool, and RV blood pool (9). The myocardial ROI enclosed the entire width of the septal myocardium, while the LV and RV blood pool ROIs were positioned centrally so as to exclude papillary muscles and trabeculations. Noise measurements were determined by placing identical ROIs outside the body in an area that was free from artifact. The SD of signal from each noise ROI was averaged across all images to give measured noise

(N_m) for the study. Effective noise (N) was determined by correcting N_m by a factor of 0.695 as reported by Henkelman (10) to account for underestimation of noise measured from magnitude images.

Since parallel imaging techniques like SENSE alter noise characteristics, noise from accelerated studies (N_{SENSE}) was estimated based on the following calculation (9):

$$N_{SENSE} = \sqrt{R} \times g \times N \quad (1)$$

where R represents the acceleration factor (R = 3 in this study), g represents the geometric factor, and N represents effective noise from the corresponding non-accelerated 3T study. The geometric factor was determined using a phantom (11) and was found to have a maximum value of 1.013.

Signal-to-noise ratios in accelerated (SNR_{SENSE}) and non-accelerated (SNR) studies were calculated by the following equation:

$$SNR = \frac{SI}{N} \quad \text{and} \quad SNR_{SENSE} = \frac{SI}{N_{SENSE}} \quad (2)$$

where SI represents signal intensity of the anatomy of interest. Signal-to-noise calculations were made for the septal myocardium (SNR_{Myo}), the LV blood pool (SNR_{LVB}) and the RV blood pool (SNR_{RVB}).

LV and RV contrast-to-noise ratios (CNR) were calculated using the following equation:

$$CNR_{LV,RV} = SNR_{LV,RV} - SNR_{Myo} \quad (3)$$

Structural and Functional Assessment

All short axis datasets were transmitted to a workstation for analysis with QMASS® Magnetic Resonance software (Version 6.2.1). Image contrast and brightness were held constant

for all analyses. Epicardial and endocardial contours were manually traced by an experienced observer in all end-diastolic and end-systolic frames. The observer was blinded to subject identity, field strength, and SENSE factor for assessment of ventricular measurements. Voxel summation was used to calculate LV and RV mass, end-systolic volume, end-diastolic volume, and stroke volume. Papillary muscles were included in mass calculations, but were excluded in chamber volume calculations. LV and RV mass were calculated from images in the end-diastolic frame.

Statistical Analysis

The mean ± SD of signal and contrast measurements were determined for each imaging protocol. Two-sided Wilcoxon sign-rank tests identified significant differences between imaging methods. For all analyses, a level of $P < 0.05$ was considered statistically significant.

Statistical significance of differences in measurement reproducibility were assessed using the Bland-Altman method (12). Differences in paired measurements between imaging methods were used to determine systematic bias (mean difference) and random error (SD of differences) associated with each method. Two-sided Wilcoxon sign-ranked tests identified significant differences in Bland-Altman reproducibility. Interstudy reproducibility was also described by coefficients of variability (13). Coefficients of variability are calculated by dividing the SD of measurement differences between two methods (Bland-Altman SD) by the population mean.

Prior studies have described interstudy reproducibility with intraclass correlation coefficients (ICC) (14). However, ICC is strongly influenced by the variance in the population from which it is assessed, and might not be comparable for different populations.

Sample sizes required to detect clinical changes in LV and RV parameters with 90% power and an α-error of 0.05 were determined using the equation (4):

$$n = f(\alpha,P) \times \sigma^2 \times 2/\delta^2 \quad (4)$$

where n represents sample size, α represents significance level (0.05), P represents power (0.90), σ represents the interstudy SD, and δ represents the measurement difference to be detected, and f represents the factor for different values of α and P (f = 10.5 when α = 0.05 and P = 0.90). All calculations were performed using SAS (Release 9.1, SAS Institute Inc., Cary, NC).

Results

MRI Completion:

All 32 subjects successfully underwent scanning at 1.5 and 3T. Population characteristics and measures of ventricular function at 1.5T are presented (Table 1). Studies from all 32 participants satisfied image quality requirements and were included in the statistical analyses. Comparable images were acquired using each method (Fig. 1). The mean scan time was 8 ± 2 min at 1.5T, 9 ± 3 min at 3T (No SENSE), and 3 ± 1 min at 3T (SENSE=3).

Signal and Contrast Assessment:

Table 2 summarizes SNR and CNR data from the study population using all 3 methods. RV blood pool SNR (SNR_{RVB}) was between 20-26% lower than LV blood pool SNR (SNR_{LVB}) for each method. Similarly, right ventricular CNR (CNR_{RV}) was between 25-31% lower than the left ventricular CNR (CNR_{LV}) as determined by each method. The largest difference between CNR_{LV} and CNR_{RV} was detected at 3T study using the non-accelerated method (84 ± 15 vs. 58 ± 12, $P < 0.001$).

Appreciable gains in SNR_{RVB} (84 ± 6 %, P < 0.001) and SNR_{LV} (94 ± 5%, P < 0.001) were observed between non-accelerated 1.5 and 3T methods, which is consistent with prior studies.(8,9) Significant gains in CNR_{RV} (75 ± 5%, P < 0.001) and CNR_{LV} (92 ± 7%, P < 0.001) were also detected between these two methods.

Gains in SNR_{RV} and SNR_{LV} between 1.5T and accelerated 3T studies were less (6 ± 3% and 13 ± 3%, respectively). CNR_{LV} increased modestly between 1.5T and accelerated 3T methods (11 ± 4%, P < 0.05), but no significant gains in CNR_{RV} were observed (1 ± 3%, P = 0.83).

Interstudy Variability:

Bland-Altman bias ± SD for LV and RV measurements are reported in along with 95% limits of agreement (Table 3). Coefficients of variability (CoV) for each analysis are also shown (Fig. 2). We observed good comparability in all LV measurements between the three imaging methods. The variability of LV measurements between two 1.5T studies was not significantly different from the variability between a 1.5T study and an accelerated 3T study with SENSE. For example, interstudy reproducibility of LV mass between two 1.5T studies (-0.3 ± 4.9 g) was comparable to the interstudy reproducibility between 1.5T and accelerated 3T studies (-0.9 ± 5.2 g,) P = 0.735 (Fig. 3a). Similarly, interstudy reproducibility of LV ejection fraction between two 1.5T studies (-0.4 ± 2.7 units) was comparable to the interstudy reproducibility between 1.5T and accelerated 3T studies (-0.8 ± 3.0 units), P = 0.884 (Fig. 3b).

RV measurements were less reproducible than corresponding LV measurements. However, no significant differences in RV measurements were detected between methods. The interstudy reproducibility of RV mass between two 1.5T studies (-1.7 ± 5.2 g) was comparable to

the reproducibility between 1.5T and accelerated 3T studies (-2.2 ± 5.8 g), P = 0.560 (Fig. 3c). Interstudy reproducibility of RV ejection fraction between two 1.5T studies (-0.4 ± 3.5 units) was comparable to the interstudy reproducibility between 1.5T and accelerated 3T studies (-0.9 ± 4.2 units), P = 0.815 (Fig. 3d).

Sample Size Calculations:

Table 4 shows sample sizes required to detect clinically important changes in cardiac parameters using serial SSFP CMR**.** Values are compared to sample size calculations previously reported by Grothues et al.(4) for serial FLASH CMR at 1.5T. For example, a sample size of 6 would be required to detect a 10 g change in LVM using serial SSFP CMR at 1.5T. However, 8 subjects would be required to detect the same change if initial SSFP studies were acquired at 1.5T and follow-up studies were acquired at 3T using SENSE.

Discussion

The results of this study indicate: (1) accelerated SSFP imaging at 3T produces comparable RV and LV contrast compared to conventional 1.5T imaging; and (2) the reproducibility of RV and LV measurements between a 1.5T study and an accelerated 3T study using SENSE is comparable to that observed between two 1.5T studies.

Cine CMR at 1.5T has been considered the gold standard for assessment of LV and RV mass and chamber volumes because of its high spatial resolution, and because it determines these measurements directly from a series of tomographic slices without making geometric assumptions (2,15). Although SSFP CMR has been performed at 3T, there has been concern that artifacts (susceptibility and others) could limit the routine use of 3T CMR for cardiac evaluation

(16). In this study we imaged individuals with and without cardiac disease at 3T with excellent results. This may be due to the continued optimization of high field strength sequences, improved local shimming and better control of center frequency compared to earlier studies. The body habitus (BSA and BMI) in this study parallels the general population in the United States (17) which suggests our results can be widely applied to clinical and population-based studies.

To our knowledge, this was the first study to evaluate both right- and left-ventricular CNR (CNR_{RV} and CNR_{LV}) using the SSFP technique. The RV is impacted in a wide range of cardiovascular diseases, and the ability to make accurate and reproducible RV measurements is of importance (18). Using conventional 1.5T CMR, CNR_{RV} was found to be approximately 25% lower than CNR_{LV}, which was attributed to lower signal intensity detected within the RV blood pool. Similarly, gains in CNR_{RV} at 3T were less robust than corresponding gains in CNR_{LV}, suggesting a restriction of RV signal intensity gains at high field strength. This is an unexpected finding since the RV is closer to the chest wall and the receiver surface coils than the LV.

One possible explanation for signal loss in the RV blood pool at 3T is an increase in dark flow artifact over the right ventricular FOV. Li et al. recently described the sensitivity of SSFP cine techniques to dark flow artifact at 1.5T, and demonstrated these artifacts were the product of small magnetic field inhomogeneities and center frequency offsets (19). At 3T these small magnetic field inhomogeneities would result in greater absolute frequency differences (6) which would be expected to lead to greater dephasing and more dark flow artifact thus restricting CNR gains. Similar to Li we observed a lower contrast-to-noise in the RV as compared to the LV in our 1.5T scans (CNR_{RV} = 33 vs. CNR_{LV} = 44). At 3T without SENSE, this difference was greater (CNR_{RV} = 58 vs CNR_{LV} = 84). If the mechanism proposed by Li is correct, the

dephasing could potentially be addressed by reducing the echo time and minimizing the absolute frequency differences across the right ventricle as much as possible.

Another possibility is that reduced oxygen tension within the RV blood pool causes T2 shortening. Since the SSFP sequence exhibits T2/T1 contrast weighting, reducing T2 of the RV blood pool would effectively decrease signal intensity (1). Blood oxygen level-dependent (BOLD) effects on T2 are well described (20), and are more significant at high field strength (21). This could also limit right ventricular CNR gains at 3T. .

Serial CMR at 1.5T using FLASH has been shown to have good interstudy reproducibility for evaluating myocardial mass and volumes in both the RV and LV (2-4,15,22,23). However, limited studies describe the interstudy reproducibility of 1.5 and 3T SSFP CMR with parallel imaging (3,4,9,24). Wintersperger et al. compared LV volumetric measurements between 1.5T and accelerated 3T studies using TSENSE, but neither myocardial mass nor RV volumetric data were presented, and only ten subjects were studied (9). Hudsmith et al. reported interstudy variability of cardiac measurements at 1.5T and 3T, but only four healthy volunteers were evaluated and parallel imaging was not used (24). Finally, Grothues et al. reported interstudy variability of LV (4) and RV (3) measurements by serial 1.5T CMR, but the study utilized a gradient echo (FLASH) sequence instead of SSFP, and the impact of 3T was not evaluated.

Interstudy variability is traditionally described by the SD of measurement differences between two studies (12) and by coefficients of variability (13). We demonstrated that the variability of LV and RV measurements between 1.5T and accelerated 3T studies was comparable to the variability between two 1.5T studies. No significant measurement differences were detected between the two methods. The study was adequately powered (>90%) to detect a

10% change in variability for each endpoint. The coefficients of variability we reported for RV and LV measurements are consistent with previously reported values (3,4). These results indicate that SSFP CMR exams performed at 1.5T and 3T with SENSE can be routinely compared for evaluation of cardiac disease progression, assuming standardized protocols are used.

Highly reproducible methods reduce the sample size required for clinical trials.(25) Currently, SSFP CMR at 1.5T is considered the accepted method for evaluating cardiac structure and function (2). To our knowledge, this was the first study to determine sample sizes required for clinical trials that wish to use serial SSFP CMR to monitor changes in LV and RV endpoints. We compared our results to sample size calculations previously established for LV parameters using FLASH CMR at 1.5T (4). Although our sample populations were different, both were similar with respect to mean age, BMI, body surface area, and LV function.

There were several limitations in this study. First, only four coil elements and receiver channels were utilized, which limited SENSE imaging to a low acceleration factor (R = 3). Additional coil elements permit the use of higher acceleration factors (9). Second, more sophisticated parallel imaging techniques have recently become available to CMR and offer the potential for greater acceleration than SENSE. Such techniques include generalized auto-calibrating partially parallel acquisitions (GRAPPA) (26) and broad-use linear acquisition speed-up technique (k-t BLAST) (27). Finally, different technologists operated the 1.5T and 3T MR systems. Thus, there was a potential for slice positioning bias between operators. We addressed this issue using a standardized clinical technique in which scout films from the initial CMR study were used as guides for co-registration of all subsequent studies. Automated repositioning

programs have become integrated into newer MR systems to minimize repositioning error; however, these programs were not available for our study.

In conclusion, we demonstrated that SSFP CMR is a very reproducible technique for evaluating RV and LV measurements. Using an acceleration factor of $R = 3$, SENSE imaging at 3 T produces CNR comparable to conventional 1.5 T imaging with a reduction in total scan time. Furthermore, the interstudy reproducibility of RV and LV measurements between a 1.5 T study and an accelerated 3 T study is comparable to the interstudy reproducibility between two 1.5T studies.

CHAPTER TWO

Assessment and Reproducibility of Aortic Atherosclerosis MR Imaging: Impact of 3-Tesla Field Strength and Parallel Imaging

Introduction

Atherosclerotic cardiovascular disease (CVD) is the leading cause of death within the United States (28-30). Recently, aortic atherosclerosis has been recognized as a risk factor for coronary artery disease and stroke (31,32). Autopsy studies have demonstrated an association between coronary artery atherosclerosis and aortic plaque burden (29,33,34). More recent studies have demonstrated the utility of magnetic resonance (MR) imaging techniques for quantifying plaque burden in the thoracic and abdominal aorta (35-37). Unlike other imaging modalities, MR offers the ability to measure plaque burden and characterize aortic plaque composition without the use of ionizing radiation (30).

Most aortic atherosclerosis imaging to date has been performed using a black-blood technique at 1.5-T (38). Recently, clinical MR at 3-T has become widely available which increases the signal obtained during imaging (39). Parallel imaging algorithms such as sensitivity encoding (SENSE) can translate this added signal into decreased scan time (40,41). Shorter acquisition times could reduce motion artifact caused by respiration and bowel peristalsis.

However, there has been concern that body imaging at 3-T would be limited by artifacts which become more prominent as field strength increases (39). Thus, there is need to evaluate

the significance of these artifacts and to determine if they affect interstudy variability in the assessment of aortic atherosclerosis (42,43).

The purpose of this study was: (1) to evaluate the impact of parallel imaging at 3-T on image quality and signal parameters of aortic atherosclerosis exams; and (2) to evaluate the interstudy reproducibility of black-blood aortic atherosclerosis imaging.

Materials and Methods

Study Participants

Twenty healthy volunteers (12 female and 8 male, mean age 51 years ± 14) and twelve patients with impaired LV function (3 female and 9 male, mean age 52 years ± 10) were recruited for this study. Of the patients with impaired LV function, 10 had angiographic evidence of coronary artery disease (CAD) and 2 were diagnosed with dilated cardiomyopathy. All patients were in sinus rhythm throughout the study. Subjects were excluded if they had any contraindication to CMR.

MR Imaging

Images were obtained using a 3-T system (Achieva; Philips Medical Systems, Best, The Netherlands) and a 1.5-T system (Achieva; Philips Medical Systems, Best, The Netherlands) which were operated by different technologists. All 32 subjects underwent four imaging studies of the abdominal aorta on the same day: Study A consisted of conventional 1.5-T imaging. Study B consisted of 3-T imaging without SENSE. Study C consisted of accelerated 3-T imaging using SENSE with an acceleration factor of R=3. Study D consisted of another conventional imaging study at 1.5-T (identical to Study A). Subjects were randomized to one of three study sequences to minimize confounding by a training effect: Study A-B-C-D, Study B-C-

A-D, or Study A-D-B-C. Between each study, subjects were ambulated between 15-30 minutes before being repositioned on the MR bed. Scout films from the initial MR study were used as guides for slice co-registration in all subsequent studies.

Four-element surface receive array coils (2 anterior, 2 posterior) placed over the subject's abdomen were used for each study. Fast gradient-echo scout images were initially used to localize the abdominal aorta in the sagittal and coronal planes. Each imaging study consisted of six transverse images of the abdominal aorta spanning from the renal arteries to the aortic bifurcation. Slice thickness was 5 mm and interslice gap was 10-mm. Black-blood images were obtained using an optimized double-inversion-recovery turbo spin-echo (TSE) sequence, with free-breathing and ECG-gating. Trigger delay was set to 125-msec after each R wave. Other imaging parameters included the following: field of view (FOV) = 264 mm × 330 mm, matrix size = 256 × 512 (in-plane resolution 1.03-mm × 0.64-mm), repetition time 3 heart beats, echo time 45 msec, and turbo spin echo factor 14. Echo train lengths were adjusted at 1.5-T and 3-T so that the total duration of signal acquisition was the same at both field strengths. All images were acquired using volume shimming at both 1.5-T and 3-T. 3-T studies with SENSE (41) were run with an acceleration factor R=3, holding all other parameters constant. All imaging was performed within standard SAR limits.

Contrast and Image Quality Assessment

All studies were evaluated in a random order by an independent observer with one year of black-blood aortic imaging experience. The observer was blinded to subject name, field strength, study date, and acceleration factor. Signal intensity (SI) measurements were determined from specified regions of interest (ROI) in the aortic wall and lumen (42). Noise measurements were determined by placing identical ROIs outside the body in an area that was

free from artifact. The SD of signal from each noise ROI was averaged across all slices to determine measured noise (N_m) of each study. Effective noise (N) was calculated by correcting N_m by a factor of 0.695, to account for underestimation of noise measured from magnitude images (44).

Since SENSE alter noise characteristics, noise from accelerated studies (N_{SENSE}) was estimated based on the following calculation: (45)

$$N_{SENSE} = \sqrt{R} \times g \times N \quad (1)$$

where R represents the acceleration factor (R=3 in this study), g represents the geometric factor, and N represents effective noise from the corresponding non-accelerated 3-T study. The geometric factor was mapped using a phantom study described elsewhere (45) and was found to have a maximum value of 1.013.

Signal-to-noise ratios in non-accelerated (SNR) and accelerated (SNR_{SENSE}) studies were calculated by the equations:

$$SNR = \frac{SI}{N} \quad \text{and} \quad SNR_{SENSE} = \frac{SI}{N_{SENSE}} \quad (2)$$

where SI represents signal intensity of the anatomy of interest. Signal-to-noise calculations were made for the aortic wall (SNR_w) and the aortic lumen (SNR_l) in both non-accelerated and accelerated studies. Wall-to-lumen contrast-to-noise ratio (CNR) was calculated by the equation:

$$CNR = SNR_w - SNR_l \quad (3)$$

A subjective image quality score was also assigned to each study by an experienced reader. The quality of each study was rated on a five-point scale (31) (5 = best image quality, excellent depiction of the aortic wall; 4 = good depiction of the aortic wall, minimal artifact in the aortic field of view; 3 = partial insufficiency in depiction of the aortic wall (< 50% of

circumference); 2 = partial insufficiency in depiction of the aortic wall (> 50% of circumference); 1 = worse image quality, completely insufficient depiction of vessel wall).

Aortic Atherosclerosis Assessment

Images were transmitted to a workstation for analysis with QMASS® Magnetic Resonance software package (Version 6.2.1, Medis Medical Imaging Systems Inc., Leiden, The Netherlands). Image contrast and brightness were held constant for all analyses, and all images were magnified to 400% of their original dimensions. Luminal and adventitial contours were manually traced in all transverse images, and atherosclerosis parameters were analyzed with the observer blinded to subject identity, field strength, and acceleration. Atherosclerotic plaque was identified by hyper-intense signal that protruded ≥ 1mm from the endoluminal surface of the aortic wall. Plaque was manually contoured in each image, and voxel summation was used to calculate the following endpoints: total vascular area (TVA) = ∑ vessel area in each slice for all slices; total luminal area (TLA) = ∑ luminal area in each slice for all slices; total wall area (TWA) = TVA – TLA; total plaque area (TPA) = ∑ plaque area in each slice for all slices; area plaque burden (APB) = 100 x (TPA / TVA); perimeter plaque burden (PPB) = 100 x (∑ plaque perimeter in each slice / ∑ endoluminal circumference in each slice); and mean aortic wall thickness (MWT) (19).

Images were included for further analysis if (1) residual flow signal was not present in greater than 50% of the lumen or (2) the imaging slice was positioned between the renal arteries the aortic bifurcation.

Statistical Analysis

The mean ± SD of contrast and image quality parameters were determined for each imaging method in the entire study population. Two-sided Wilcoxon signed-rank tests were used

to identify significant differences between imaging methods ($P < 0.05$ was considered significant).

Interstudy reproducibility between two imaging methods was assessed using the Bland-Altman technique (47). Differences in paired measurements between the two methods were used to determine systematic error (Bland-Altman mean) and random error (Bland-Altman SD). To evaluate whether interstudy reproducibility between two methods was comparable to the interstudy reproducibility between two different methods, two-sided Wilcoxon signed-ranked tests were used to identify significant differences in Bland-Altman means ($P < 0.05$ was considered significant). The study was sufficiently powered (> 90%) to detect a 10% change in variability for each endpoint. All calculations were performed using SAS (Release 9.1, SAS Institute Inc., Cary, NC).

Interstudy reproducibility was also described by coefficients of variability. Coefficients of variability were calculated by dividing the SD of measurement differences between two methods (Bland-Altman SD) by the population mean.

Sample sizes required to detect clinical changes with 90% power and an α-error of 0.05 were determined by the following equation: (49)

$$n = f(\alpha,P) \times \sigma^2 \times 2/\delta^2 \qquad (4)$$

where n is the sample size, α is the significance level (0.05), P is the power (0.90), σ is the Bland-Altman SD, δ is the measurement difference to be detected, and f is an adjustment factor ($f = 10.5$ when $\alpha = 0.05$ and $P = .90$).

Results

A description of patient demographics is presented (Table 5)**.** All 32 subjects were successfully scanned at 1.5-T and 3-T. Approximately 94% of the images (722 of 768) met criteria for analysis. Comparable images were acquired by each method (Figure 5). The mean scan time was 5 min ± 2 at 1.5-T, 6 min ± 3 at 3-T (No SENSE), and 2 min ± 1 at 3-T (SENSE=3).

Contrast and Image Quality Assessment

Comparing 1.5-T studies to non-accelerated 3-T studies, significantly greater values for aortic wall SNR (11.3 ± 1.6 vs. 19.4 ± 1.9, $P < .05$) and aortic CNR (10.1 ± 1.4 vs. 17.4 ± 2.0, $P < 0.05$) were observed (Table 6). These gains paralleled increases in image quality score between 1.5-T and non-accelerated 3-T studies (4.0 ± 0.6 vs. 4.4 ± 0.5, $P < 0.05$). However, when comparing 1.5-T studies to accelerated 3-T studies (SENSE=3), no significant differences in aortic CNR (10.1 ± 1.4 vs. 10.0 ± 1.4, $P = 0.89$) or image quality score (4.0 ± 0.6 vs. 4.2 ± 0.7, $P = 0.72$) were detected.

Aortic Atherosclerosis Assessment

Bland-Altman mean ± SD for atherosclerosis measurements are reported along with 95% limits of agreement (Table 7)**.** Coefficients of variability (CoV) are also reported for each interstudy comparison (Figure 6). Bland-Altman reproducibility of area plaque burden (APB) between two 1.5-T studies (-0.02 ± 0.32 %) was comparable to the reproducibility between 1.5-T and accelerated 3-T studies (0.11 ± 0.33 %), $P = 0.29$ (Figure 7a). Bland-Altman reproducibility of mean wall thickness (MWT) between two 1.5-T studies (-0.03 mm ± 0.09) was comparable to the reproducibility between 1.5-T and accelerated 3-T studies (-0.01 mm ± 0.12), $P = .83$ (Figure 7b).

Sample sizes required to detect clinically significant changes in aortic atherosclerosis using serial black-blood MR are reported (Table 8). For example, a sample size of 8 would be required to detect a 0.25-mm change in aortic MWT using serial 1.5-T MR (assuming 90% power, α-error of 0.05). However, 10 subjects would be required to detect the same change if the first exam was performed at 1.5-T and the follow-up exam was performed at 3-T using SENSE.

Discussion

The results of this study indicate: (1) accelerated black-blood imaging of the abdominal aorta at 3-T produces comparable image quality and wall-to-lumen CNR compared to conventional 1.5-T imaging; and (2) the reproducibility of aortic atherosclerosis measurements between a 1.5-T exam and an accelerated 3-T exam using SENSE is comparable to the measurement reproducibility between two 1.5-T exams

The need to measure atherosclerosis burden has become an important component of cardiovascular risk stratification. Aortic atherosclerosis has been recognized as a risk factor for coronary artery disease and stroke (31,32). Studies have demonstrated that atherosclerotic burden is more extensive in the abdominal aorta than in other vascular beds, and develops at an early age (32,36). Black-blood MRI of the abdominal aorta is an attractive screening modality for identifying rapid plaque progressors during the asymptomatic stage of atherosclerosis, allowing for appropriate treatments and interventions to be initiated early (36).

Aortic atherosclerosis can be assessed in several ways. Quantifying the extent of raised plaque has been used widely, as it is thought to be a direct measure of disease burden and an indicator of disease progression (32,50,51). However, as raised atherosclerotic lesions may take

several decades to develop, vessel wall thickening occurs earlier (52-54). For these reasons, we evaluated interstudy reproducibility for both the extent of raised plaque and mean wall thickness.

Prior studies have demonstrated that at black-blood MR at 1.5-T is feasible for quantifying aortic atherosclerosis with high interobserver agreement (31,36,51). With the greater availability of 3-T systems, there has been considerable interest in vascular and atherosclerosis imaging at 3-T (42,43). Koops et al. recently demonstrated that 3-T aortic imaging in cadavers could successfully characterize plaque extent and composition with good correlation to histopathology (31). The additional signal afforded by 3-T can be translated into acceleration using parallel imaging algorithms such as SENSE (41).

To our knowledge, this is the first study to report signal and contrast parameters of the abdominal aorta using T2-weighted black-blood MRI at 1.5-T and 3-T. We observed a mean 71% increase in the aortic wall SNR and a mean 72% increase in wall-to-lumen CNR between 1.5-T and non-accelerated 3-T studies. These results are similar to those reported by Yarnykh et al. in their evaluation of carotid arteries at 1.5-T and 3-T (42). Signal and contrast measurements acquired at 3-T with SENSE were highly comparable to measurements acquired using the conventional 1.5-T method. At this time it is unknown whether greater accelerations can be achieved with arrays with more than 4 coils although preliminary reports suggest that this may be possible (40,41).

In a prior study, Koops et al described scored image quality of the abdominal aorta in cadavers at 1.5-T and 3-T (31). We used the same scoring criteria in our assessment of image quality. Changes in image quality between methods paralleled changes in aortic CNR, as shown in Table 6. A significant increase in image quality was detected between 1.5-T and non-accelerated 3-T studies, but no significant differences were detected between 1.5-T and

accelerated 3-T studies. Since 3-T imaging with SENSE produces comparable CNR to 1.5-T imaging with a significant reduction in total scan time, less motion artifact could occur with the accelerated technique. which could explain the somewhat superior image quality reported at 3-T with SENSE compared to 1.5-T.

Good interstudy reproducibility is crucial if MR is to be monitor plaque progression and response to therapy (49). Chan et al. investigated interstudy reproducibility of aortic atherosclerosis imaging using MR (51). However, this study was limited by a comparatively small sample size and limited statistical measures of reproducibility. Further, the group did not investigate effects of 3-T and parallel imaging algorithms on measurement reproducibility.

Our study demonstrated good reproducibility of aortic atherosclerosis measurements between 1.5-T and 3-T studies using SENSE. This reproducibility was comparable to measurement reproducibility between two 1.5-T exams. We also demonstrated that SENSE imaging at 3-T reduces scan time by approximately 60% compared to conventional 1.5-T imaging. We found interstudy reproducibility of mean wall thickness (MWT) to be particularly high between the two imaging methods suggesting this parameter would be an ideal endpoint for following changes in aortic atherosclerosis. Prior results from the Multiethnic Study of Atherosclerosis demonstrated excellent interobserver agreement in measuring mean wall thickness. Our ability to detect small changes in wall thickness during the subclinical stages of atherosclerosis could help identify patients at risk for developing vulnerable plaque and ischemic events later in life.

Several clinical trials have evaluated the effects of lipid-lowering therapies on aortic atherosclerosis using serial 1.5-T MR (53-55). Knowledge of the sample size required to detect a clinically significant change in atherosclerosis can ensure the proper design of interventional

studies. We reported sample sizes required to detect clinically significant changes in aortic atherosclerosis with 90% power (assuming an α-error of 0.05) (53,54). For example, an estimated sample size of just 8-10 subjects would be required to detect a clinically significant change in MWT using serial MRI.

There were several limitations to this study. First, this study did not evaluate plaque composition. Although black-blood MRI has the capability to distinguish various plaque constituents (lipid core, fibrous cap, calcification), this requires multi-contrast acquisitions which was not the focus of the present investigation (30,56). Second, only six images of the infrarenal abdominal aorta were acquired as has been done in other studies. Thus, some subclinical atherosclerosis could have been missed. The time saving achieved with SENSE could be used to obtain more slices and reduce the potential for missing disease. Third, only four coil elements and receiver channels were used in our study, which limited SENSE imaging to a low acceleration factor. Additional coil elements can potentially allow for higher accelerations without compromising SNR (41). Finally, a manual contouring program was used to detect vessel boundaries in each study. Recently, semi-automated image processing tools have been developed that allow for further refinement of interstudy reproducibility (52), but such programs were not available for our study.

In conclusion, we demonstrated that accelerated black-blood MR imaging at 3-T is a reliable technique for monitoring atherosclerosis burden in the abdominal aorta. Using an acceleration factor of R=3, SENSE imaging at 3-T produces comparable image quality and vessel contrast compared to conventional 1.5-T methods. Furthermore, the reproducibility of aortic plaque measurements between two 1.5-T studies is comparable to the reproducibility between a 1.5-T and an accelerated 3-T study with SENSE.

CHAPTER THREE

Coronary Sinus Flow Reserve in Response to Cold Pressor Stress

A Feasibility Study in At-Risk Women

Introduction

Coronary sinus (CS) flow estimates left ventricular (LV) coronary blood flow because the CS drains over 96% of the LV myocardium (58). Quantification of CS flow in response to pharmacologic stress has also been used as a surrogate measure of coronary flow reserve (CFR) (58-62) and the function of coronary microvasculature (63-65). Several techniques have interrogated CS flow to measure CFR, including continuous thermodilution (66) and transesophageal echocardiography (TEE) (67). However, widespread clinical use of these techniques is limited by their invasiveness. Velocity-encoded cine (VEC) magnetic resonance imaging (MRI) of the CS was first developed by van Rossum et al.(61) as a noninvasive technique for measuring CS flow and CFR. Several studies have demonstrated the ability of CS VEC MRI to measure CFR in patients with heart failure (58,59), LV hypertrophy (62), and dilated cardiomyopathy (60) at 1.5 Tesla.

A noninvasive measurement of CFR may be particularly helpful in identifying and treating symptomatic and asymptomatic women at increased risk for cardiac events. Invasive measurements of CFR have been shown to be an independent predictor of cardiac morbidity (65,66) and predict events in symptomatic women before angiographic evidence of obstructive disease (69-71). However, imaging women at risk for cardiovascular disease is often challenging due to their larger body size and smaller coronary arteries (72,73). Therefore, we

chose to test the feasibility of CS flow imaging in overweight and obese women to determine whether significant changes in CS flow were detectable at 3 Tesla, taking advantage of higher signal-to-noise afforded by increased field strength. A spiral k-space sampling method also allowed for improved spatial and temporal resolution with less sensitivity to motion artifact (74). The cold pressor test (CPT) was utilized instead of pharmacologic stress because it evokes an endothelium-dependent coronary vasodilation that may be more sensitive to early signs of atherosclerosis before the development of obstructive disease (65,70,75). CS flow changes after CPT were also compared to flow changes in the right coronary artery (RCA) to determine if cold stress provokes similar responses in these target vessels.

The goals of this study were: (1) to evaluate feasibility of stress CS flow imaging by spiral VEC MRI at 3 Tesla in overweight women with cardiovascular risk factors; (2) to determine if significant changes in CS flow are detectable in response to the CPT; and (3) to compare changes in CS flow to changes in the right coronary artery (RCA).

Methods

Participants:

This study was approved by the local Institutional Review Board, and all participants provided written informed consent. Ten overweight or obese females (age 38 years ± 10) were recruited who were premenopausal and had no history of obstructive coronary artery disease, stroke, lung disease, hypertension, and no current tobacco or cocaine use. Participants were excluded from the study if they had any contraindication to MR imaging.

Cardiac MRI Technique:

All images were acquired with a 3 Tesla MR scanner (Achieva, Philips, Netherlands). Data was acquired with a 6-element cardiac receiver coil with the subject in the supine position. Retrospective electrocardiographic gating was utilized. For cardiac orientation, scout images were acquired in three orthogonal planes using a balanced turbo field echo (B-TFE) sequence. Axial B-TFE images of the heart were obtained through the atrioventricular groove to identify the CS. A single imaging plane was selected perpendicular to the CS at a 3-cm distance from the ostium. The 3-D orientation of the proximal RCA was localized using a free-breathing navigator B-TFE sequence from which a perpendicular imaging plane was selected for flow imaging.

VEC MRI

Baseline CS flow was acquired using a VCG triggered end-expiratory breath-hold (11-15 sec) spiral VEC sequence with the following parameters: TR/TE 34/3.5 msec, RF excitation angle 20^{o}, FOV 250 × 250 mm^2, spatial resolution 0.8 × 0.8 × 7 mm^3, temporal resolution 69 msec, VENC 80 cm/sec, spiral interleaves 11. Baseline RCA flow was acquired using the same end-expiratory breath-hold sequence with the following exception: VENC 35 cm/sec.

In each flow imaging series, 12-14 phases of data were acquired and reconstructed into velocity and magnitude images.

Cold Pressor Test

After baseline flow was measured, the participant's left hand was immersed in an ice water bath (50% ice, 50% water) for 3 minutes. Repeat flow images of the CS and RCA were acquired immediately following CPT, and again at 1-min, 5-min, and 10-mins post-CPT. BP and HR were recorded at baseline and at 30 sec intervals throughout the study.

Image Analysis

Phase and magnitude images were transferred to a remote workstation and analyzed using QFLOW (v. 4.1.6, Medis, Leesburg, VA). Vessel contours were manually traced on each magnitude image by two trained observers (CM and AC). Identical tracings were automatically applied to the corresponding phase images so that mean volume flow (ml/sec) and flow velocity (cm/sec) in the CS could be determined. Mean volume flow was derived from the integration of phasic flow over time. Coronary flow reserve was calculated by diving CS volume flow during peak stress by CS volume flow at rest.

Flow through the RCA was measured using the same technique. Peak flow velocity during diastole in the RCA was the measurement selected to represent RCA flow (76,77). All datasets were acquired in duplicate at each time interval, and the mean value was reported.

Statistical Analysis

Data are expressed as mean plus or minus standard deviation (SD). Differences before and after cold pressor stress were analyzed by means of a *t* test for paired data. Linear regression was used for correlation analysis. A *p* value of less than 0.05 was considered to indicate statistical significance. Inter-observer variability was determined using Bland-Altman analysis.

Results

All ten participants tolerated CPT, and successful CS flow images were acquired at baseline and after stress (Figure 8). The sample of women were ethnically diverse, had a mean BMI of 33 $kg/m^2 \pm 8$ and included women with previously diagnosed type 2 diabetes, lipid abnormalities, family history of coronary artery disease, and past history of tobacco use (Table 9).

CS Flow at Rest and After Cold Pressor Stress

Figure 9 shows representative tracings of CS volume flow, flow velocity, and cross-sectional area throughout the cardiac cycle at rest and following cold pressor stress. Flow tracings demonstrate bimodal flow peaks: one during systole and another during diastole. CS area varied throughout the cardiac cycle, noticeably more during peak stress. CS area increased by 12 % ± 7 from rest to peak cold pressor stress, but this change was not significant.

A significant 45% increase in rate-pressure product was observed from rest to peak cold pressor stress (6947 ± 954 mmHg/min vs 10,033 ± 2039 mmHg/min, $p < 0.01$), as shown in Table 10. Significant increases in CS volume flow (141 ± 34 ml/min vs 184 ± 42 ml/min, $p = 0.02$) and CS flow velocity (11.0 ± 4.0 cm/sec vs 16.3 ± 5.7 cm/sec, $p = 0.02$) were also observed from rest to peak cold pressor stress. CS volume flow at baseline, during cold stress, and during recovery are presented in Figure 10. Coronary flow reserve in response to cold pressor stress was 1.33 ± 0.08.

Inter-observer variability of CS volume flow was 1% ± 7 during rest and 1% ± 6 during stress, suggesting improved reliability compared to previously reported techniques at 1.5 Tesla (58,60,78).

Relationship Between CS Flow and RCA Flow

RCA flow velocity increased 56% ± 37 from rest to peak stress, and CS volume flow increased 24% ± 8 from rest to peak stress. Flow velocity through the RCA correlated strongly with CS volume flow at baseline ($r = 0.94$), and also during peak cold pressor stress ($r = 0.86$), as depicted in Figure 11.

Discussion

The results of this study demonstrate that: (1) spiral VEC MRI at 3T can measure significant changes in CS flow in overweight and obese women and (2) significant changes in CS flow are detectable with the non-pharmacologic stress of CPT.

Our data are in agreement with previous observations of 30-40% increase in myocardial blood flow and coronary artery blood flow in healthy subjects after cold pressor stress (65,79). Although increases in coronary flow are less robust with CPT than with pharmacologic stressors like adenosine and dipyramidole (3- to 5-fold augmentation in flow) (77), a significant increase in CS flow was observed in our study group of women despite their larger body size and smaller vessels. Flow tracings demonstrate bimodal flow peaks: one during systole and another during diastole, which is in agreement with previously reported data (59,61,79,80). CS area increased by 20% during CPT which is similar to prior studies using pharmacologic stress (58,61,80) and suggests a limit to the capacitance function of cardiac venous outflow.

To our knowledge, this is the first study to (1) investigate the feasibility of VEC MR flow imaging of the CS at 3 Tesla and (2) to use the spiral acquisition technique to measure CS flow. The increased field strength afforded by 3 Tesla yields greater tissue signal, which can be exchanged for increased resolution and accelerated acquisition speed (74). Such improvements are advantageous for coronary imaging because of small vessel size (several millimeters in diameter) and motion of the heart and diaphragm. Furthermore, this was the first study to apply a 3D spiral acquisition technique to flow imaging in the CS. Spiral imaging is less sensitive to motion than Cartesian trajectories because the center of k-space is oversampled, allowing for phase correction between various lines of acquired data (81). Bansmann et al. previously

showed that RCA vessel wall imaging with spiral k-space technique yields higher signal-to-noise ratios with less motion artifact than Cartesian sampling at 3 Tesla (74).

VEC MRI can be used to quantify CFR by measuring (1) changes in coronary arterial flow in response to stress, or (2) changes in CS flow in response to stress. Although both techniques have been reported, their feasibility and clinical applications differ. The CS is an attractive alternative for quantifying coronary volume flow because: (1) it is larger (> 8 mm in diameter), (2) there is less turbulent blood flow at its luminal margins, and (3) it has a more predictable anatomic location and course (61,82). These criteria contribute to the improved vessel border conspicuity of the CS and reduce intravoxel averaging of blood flow measurements. Furthermore, since the CS drains the majority of LV blood, measuring CFR from CS flow can provide valuable information about diffuse cardiovascular processes such as coronary microvascular disease (63,80), which may be detectable or symptomatic before large vessel epicardial disease. CFR measurements acquired directly from a coronary artery may be less sensitive to early deficits in microvascular perfusion. Direct coronary artery flow imaging is most appropriate for assessing the significance of a known stenotic lesion (76,77).

Quantification of blood flow in a coronary artery is challenging because of small vessel size (3-4 mm in diameter) and considerable cardiac and respiratory motion (76). Intravoxel averaging of flowing blood signal and insufficient temporal resolution have limited the accuracy of direct volume flow measurements in the coronary arteries. In light of these limitations, flow velocity reserve has emerged as a surrogate for CFR in the coronary arteries, since flow velocity measurements are less sensitive to errors in vessel wall measurement (77). Our study demonstrated good correlation between flow velocity changes in the RCA and flow volume changes in the CS in response to endothelium-dependent stress.

The advantage of CPT is that it focuses on an endothelium-dependent response via a centrally-mediated sympathetic response that is non-pharmacologic (63,75,79). CPT may also be able to detect subclinical coronary atherosclerosis. Recent studies demonstrated that endothelium-dependent coronary vasodilation is impaired in patients with diabetes and cardiovascular risk factors, even in the absence of epicardial artery lesions (69,83,84). In addition, we found that it was not necessary to adjust velocity encoding settings during CPT, as no aliasing was observed in phase-encoded images.

Limitations

First, this small study was limited in its ability to explore the impact of individual cardiac risk factors on CFR in response to CPT. Second, myocardial mass and LV function were not determined in our subjects. Therefore, we cannot comment on global LV myocardial perfusion. However, differences in LV mass are less likely to contribute to variability among the women sampled who did not have heart failure or hypertension (77,78). Third, through-plane motion of the CS likely resulted in subtle misalignment of flow encoding, particularly during systolic phases of the cardiac cycle. However, since CS flow is integrated throughout the cardiac cycle, the net effect of cardiac motion was minimized because cardiac contraction and relaxation are associated with opposing velocity vectors (77). Finally, susceptibility artifacts and off-resonance effects were difficult to completely eliminate in this study, but they did not appear to significantly interfere with flow measurements in the CS and RCA. Reported flow measurements are consistent with previously published data (59-61).

CHAPTER FOUR

Conclusions & Recommendations

These research studies have demonstrated that SSFP CMR is a reproducible technique for evaluating right and left ventricular measurements. Using an acceleration factor of $R = 3$, SENSE imaging at 3T produces CNR comparable to conventional 1.5T imaging with a reduction in total scan time. In addition, the interstudy reproducibility of RV and LV measurements between a 1.5 T study and an accelerated 3 T study is comparable to the interstudy reproducibility between two 1.5T studies, suggesting the 3T technique is suitable for prospective research studies and clinical application.

Our aortic atherosclerosis imaging studies demonstrated that accelerated black-blood MR imaging at 3T is a reliable technique for monitoring atherosclerosis burden in the abdominal aorta. As we observed with SSFP cardiac imaging, SENSE imaging at 3T produces comparable abdominal aorta image quality and vessel contrast compared to conventional 1.5T methods. Likewise, the reproducibility of aortic plaque measurements between two 1.5-T studies is comparable to the reproducibility between a 1.5-T and an accelerated 3-T study with SENSE.

Finally, coronary sinus spiral VEC MRI at 3 Tesla is a feasible technique for measuring changes in CS flow in overweight women with risk factors for cardiovascular disease. The cold pressor test evokes a significant increase in CS flow that may be suitable for evaluating coronary microvascular dysfunction in this population. Future studies will examine the prognostic and diagnostic utility of this technique in asymptomatic women with various cardiovascular risk factors.

BIBLIOGRAPHY

1. Barkhausen J, Ruehm SG, Goyen M, Buck T, Laub G, Debatin JF. MR evaluation of ventricular function: true fast imaging with steady-state precession versus fast low-angle shot cine MR imaging: feasibility study. Radiology 2001;219(1):264-269.
2. Moon JC, Lorenz CH, Francis JM, Smith GC, Pennell DJ. Breath-hold FLASH and FISP cardiovascular MR imaging: left ventricular volume differences and reproducibility. Radiology 2002;223(3):789-797.
3. Grothues F, Moon JC, Bellenger NG, Smith GS, Klein HU, Pennell DJ. Interstudy reproducibility of right ventricular volumes, function, and mass with cardiovascular magnetic resonance. American heart journal 2004;147(2):218-223.
4. Grothues F, Smith GC, Moon JC, Bellenger NG, Collins P, Klein HU, Pennell DJ. Comparison of interstudy reproducibility of cardiovascular magnetic resonance with two-dimensional echocardiography in normal subjects and in patients with heart failure or left ventricular hypertrophy. The American journal of cardiology 2002;90(1):29-34.
5. Kuhl HP, van der Weerdt A, Beek A, Visser F, Hanrath P, van Rossum A. Relation of end-diastolic wall thickness and the residual rim of viable myocardium by magnetic resonance imaging to myocardial viability assessed by fluorine-18 deoxyglucose positron emission tomography. The American journal of cardiology 2006;97(4):452-457.
6. Gutberlet M, Noeske R, Schwinge K, Freyhardt P, Felix R, Niendorf T. Comprehensive cardiac magnetic resonance imaging at 3.0 Tesla: feasibility and implications for clinical applications. Investigative radiology 2006;41(2):154-167.

7. Pruessmann KP, Weiger M, Scheidegger MB, Boesiger P. SENSE: sensitivity encoding for fast MRI. Magn Reson Med 1999;42(5):952-962.
8. Gutberlet M, Schwinge K, Freyhardt P, Spors B, Grothoff M, Denecke T, Ludemann L, Noeske R, Niendorf T, Felix R. Influence of high magnetic field strengths and parallel acquisition strategies on image quality in cardiac 2D CINE magnetic resonance imaging: comparison of 1.5 T vs. 3.0 T. European radiology 2005;15(8):1586-1597.
9. Wintersperger BJ, Bauner K, Reeder SB, Friedrich D, Dietrich O, Sprung KC, Picciolo M, Nikolaou K, Reiser MF, Schoenberg SO. Cardiac steady-state free precession CINE magnetic resonance imaging at 3.0 tesla: impact of parallel imaging acceleration on volumetric accuracy and signal parameters. Investigative radiology 2006;41(2):141-147.
10. Henkelman RM. Measurement of signal intensities in the presence of noise in MR images. Medical physics 1985;12(2):232-233.
11. Reeder SB, Wintersperger BJ, Dietrich O, Lanz T, Greiser A, Reiser MF, Glazer GM, Schoenberg SO. Practical approaches to the evaluation of signal-to-noise ratio performance with parallel imaging: application with cardiac imaging and a 32-channel cardiac coil. Magn Reson Med 2005;54(3):748-754.
12. Bland JM, Altman DG. Statistical methods for assessing agreement between two methods of clinical measurement. Lancet 1986;1(8476):307-310.
13. Quan H, Shih WJ. Assessing reproducibility by the within-subject coefficient of variation with random effects models. Biometrics 1996;52(4):1195-1203.
14. Yarnykh VL, Terashima M, Hayes CE, Shimakawa A, Takaya N, Nguyen PK, Brittain JH, McConnell MV, Yuan C. Multicontrast black-blood MRI of carotid arteries:

comparison between 1.5 and 3 tesla magnetic field strengths. J Magn Reson Imaging 2006;23(5):691-698.

15. Semelka RC, Tomei E, Wagner S, Mayo J, Kondo C, Suzuki J, Caputo GR, Higgins CB. Normal left ventricular dimensions and function: interstudy reproducibility of measurements with cine MR imaging. Radiology 1990;174(3 Pt 1):763-768.

16. Hinton DP, Wald LL, Pitts J, Schmitt F. Comparison of cardiac MRI on 1.5 and 3.0 Tesla clinical whole body systems. Investigative radiology 2003;38(7):436-442.

17. Victor RG, Haley RW, Willett DL, Peshock RM, Vaeth PC, Leonard D, Basit M, Cooper RS, Iannacchione VG, Visscher WA, Staab JM, Hobbs HH. The Dallas Heart Study: a population-based probability sample for the multidisciplinary study of ethnic differences in cardiovascular health. The American journal of cardiology 2004;93(12):1473-1480.

18. Zehender M, Kasper W, Kauder E, Schonthaler M, Geibel A, Olschewski M, Just H. Right ventricular infarction as an independent predictor of prognosis after acute inferior myocardial infarction. The New England journal of medicine 1993;328(14):981-988.

19. Li W, Storey P, Chen Q, Li BS, Prasad PV, Edelman RR. Dark flow artifacts with steady-state free precession cine MR technique: causes and implications for cardiac MR imaging. Radiology 2004;230(2):569-575.

20. Fieno DS, Shea SM, Li Y, Harris KR, Finn JP, Li D. Myocardial perfusion imaging based on the blood oxygen level-dependent effect using T2-prepared steady-state free-precession magnetic resonance imaging. Circulation 2004;110(10):1284-1290.

21. Parkes LM, Schwarzbach JV, Bouts AA, Deckers RH, Pullens P, Kerskens CM, Norris DG. Quantifying the spatial resolution of the gradient echo and spin echo BOLD response at 3 Tesla. Magn Reson Med 2005;54(6):1465-1472.

22. Nesser HJ, Tkalec W, Patel AR, Masani ND, Niel J, Markt B, Pandian NG. Quantitation of right ventricular volumes and ejection fraction by three-dimensional echocardiography in patients: comparison with magnetic resonance imaging and radionuclide ventriculography. Echocardiography (Mount Kisco, NY 2006;23(8):666-680.

23. Semelka RC, Tomei E, Wagner S, Mayo J, Caputo G, O'Sullivan M, Parmley WW, Chatterjee K, Wolfe C, Higgins CB. Interstudy reproducibility of dimensional and functional measurements between cine magnetic resonance studies in the morphologically abnormal left ventricle. American heart journal 1990;119(6):1367-1373.

24. Hudsmith LE, Petersen SE, Tyler DJ, Francis JM, Cheng AS, Clarke K, Selvanayagam JB, Robson MD, Neubauer S. Determination of cardiac volumes and mass with FLASH and SSFP cine sequences at 1.5 vs. 3 Tesla: a validation study. J Magn Reson Imaging 2006;24(2):312-318.

25. Bellenger NG, Davies LC, Francis JM, Coats AJ, Pennell DJ. Reduction in sample size for studies of remodeling in heart failure by the use of cardiovascular magnetic resonance. J Cardiovasc Magn Reson 2000;2(4):271-278.

26. Griswold MA, Jakob PM, Heidemann RM, Nittka M, Jellus V, Wang J, Kiefer B, Haase A. Generalized autocalibrating partially parallel acquisitions (GRAPPA). Magn Reson Med 2002;47(6):1202-1210.

27. Kozerke S, Tsao J, Razavi R, Boesiger P. Accelerating cardiac cine 3D imaging using k-t BLAST. Magn Reson Med 2004;52(1):19-26.

28. Serfaty JM, Chaabane L, Tabib A, Chevallier JM, Briguet A, Douek PC. Atherosclerotic plaques: classification and characterization with T2-weighted high-spatial-resolution MR imaging-- an in vitro study. Radiology 2001; 219:403-410.

29. McMahan CA, Gidding SS, Fayad ZA, et al. Risk scores predict atherosclerotic lesions in young people. Arch Intern Med 2005; 165:883-890.

30. Yuan C, Kerwin WS. MRI of atherosclerosis. J Magn Reson Imaging 2004; 19:710-719.

31. Koops A, Ittrich H, Petri S, et al. Multicontrast-weighted magnetic resonance imaging of atherosclerotic plaques at 3.0 and 1.5 Tesla: ex-vivo comparison with histopathologic correlation. Eur Radiol 2007; 17:279-286.

32. Taniguchi H, Momiyama Y, Fayad ZA, et al. In vivo magnetic resonance evaluation of associations between aortic atherosclerosis and both risk factors and coronary artery disease in patients referred for coronary angiography. Am Heart J 2004; 148:137-143.

33. McGill HC, Jr., McMahan CA, Herderick EE, et al. Effects of coronary heart disease risk factors on atherosclerosis of selected regions of the aorta and right coronary artery. PDAY Research Group. Pathobiological Determinants of Atherosclerosis in Youth. Arterioscler Thromb Vasc Biol 2000; 20:836-845.

34. Strong JP, Malcom GT, McMahan CA, et al. Prevalence and extent of atherosclerosis in adolescents and young adults: implications for prevention from the Pathobiological Determinants of Atherosclerosis in Youth Study. Jama 1999; 281:727-735.

35. Victor RG, Haley RW, Willett DL, et al. The Dallas Heart Study: a population-based probability sample for the multidisciplinary study of ethnic differences in cardiovascular health. Am J Cardiol 2004; 93:1473-1480.

36. Jaffer FA, O'Donnell CJ, Larson MG, et al. Age and sex distribution of subclinical aortic atherosclerosis: a magnetic resonance imaging examination of the Framingham Heart Study. Arterioscler Thromb Vasc Biol 2002; 22:849-854.

37. Li AE, Kamel I, Rando F, et al. Using MRI to assess aortic wall thickness in the multiethnic study of atherosclerosis: distribution by race, sex, and age. AJR Am J Roentgenol 2004; 182:593-597.

38. Simonetti OP, Finn JP, White RD, Laub G, Henry DA. "Black blood" T2-weighted inversion-recovery MR imaging of the heart. Radiology 1996; 199:49-57.

39. Hinton DP, Wald LL, Pitts J, Schmitt F. Comparison of cardiac MRI on 1.5 and 3.0 Tesla clinical whole body systems. Invest Radiol 2003; 38:436-442.

40. Kramer H, Schoenberg SO, Nikolaou K, et al. Cardiovascular screening with parallel imaging techniques and a whole-body MR imager. Radiology 2005; 236:300-310.

41. Pruessmann KP, Weiger M, Scheidegger MB, Boesiger P. SENSE: sensitivity encoding for fast MRI. Magn Reson Med 1999; 42:952-962.

42. Yarnykh VL, Terashima M, Hayes CE, et al. Multicontrast black-blood MRI of carotid arteries: comparison between 1.5 and 3 tesla magnetic field strengths. J Magn Reson Imaging 2006; 23:691-698.

43. Nael K, Ruehm SG, Michaely HJ, et al. High spatial-resolution CE-MRA of the carotid circulation with parallel imaging: comparison of image quality between 2 different acceleration factors at 3.0 Tesla. Invest Radiol 2006; 41:391-399.

44. Henkelman RM. Measurement of signal intensities in the presence of noise in MR images. Med Phys 1985; 12:232-233.

45. Reeder SB, Wintersperger BJ, Dietrich O, et al. Practical approaches to the evaluation of signal-to-noise ratio performance with parallel imaging: application with cardiac imaging and a 32-channel cardiac coil. Magn Reson Med 2005; 54:748-754.

46. Rosero EB, Timaran CH, Khera A, Lo HS, Peshock R. Abdominal Aortic Wall-Thickness by Magnetic Resonance Imaging and Cardiovascular Disease in a Multi-ethnic Population-Based Study. UT Southwestern Clin Res Symposium 2007; Apr 2007.

47. Bland JM, Altman DG. Statistical methods for assessing agreement between two methods of clinical measurement. Lancet 1986; 1:307-310.

48. Quan H, Shih WJ. Assessing reproducibility by the within-subject coefficient of variation with random effects models. Biometrics 1996; 52:1195-1203.

49. Grothues F, Smith GC, Moon JC, et al. Comparison of interstudy reproducibility of cardiovascular magnetic resonance with two-dimensional echocardiography in normal subjects and in patients with heart failure or left ventricular hypertrophy. Am J Cardiol 2002; 90:29-34.

50. Kim WY, Astrup AS, Stuber M, et al. Subclinical coronary and aortic atherosclerosis detected by magnetic resonance imaging in type 1 diabetes with and without diabetic nephropathy. Circulation 2007; 115:228-235.

51. Chan SK, Jaffer FA, Botnar RM, et al. Scan reproducibility of magnetic resonance imaging assessment of aortic atherosclerosis burden. J Cardiovasc Magn Reson 2001; 3:331-338.

52. Glagov S, Weisenberg E, Zarins CK, Stankunavicius R, Kolettis GJ. Compensatory enlargement of human atherosclerotic coronary arteries. N Engl J Med 1987; 316:1371-1375.

53. Corti R, Fuster V, Fayad ZA, et al. Effects of aggressive versus conventional lipid-lowering therapy by simvastatin on human atherosclerotic lesions: a prospective,

randomized, double-blind trial with high-resolution magnetic resonance imaging. J Am Coll Cardiol 2005; 46:106-112.

54. Corti R, Fuster V, Fayad ZA, et al. Lipid lowering by simvastatin induces regression of human atherosclerotic lesions: two years' follow-up by high-resolution noninvasive magnetic resonance imaging. Circulation 2002; 106:2884-2887.

55. Helft G, Worthley SG, Fuster V, et al. Progression and regression of atherosclerotic lesions: monitoring with serial noninvasive magnetic resonance imaging. Circulation 2002; 105:993-998.

56. Saam T, Cai J, Ma L, et al. Comparison of symptomatic and asymptomatic atherosclerotic carotid plaque features with in vivo MR imaging. Radiology 2006; 240:464-472.

57. Ladak HM, Thomas JB, Mitchell JR, Rutt BK, Steinman DA. A semi-automatic technique for measurement of arterial wall from black blood MRI. Med Phys 2001; 28:1098-1107.

58. Lund GK, Watzinger N, Saeed M, Reddy GP, Yang M, Araoz PA, Curatola D, Bedigian M, Higgins CB: Chronic heart failure: global left ventricular perfusion and coronary flow reserve with velocity-encoded cine MR imaging: initial results. Radiology 2003, 227(1):209-215.

59. Aras A, Anik Y, Demirci A, Balci NC, Kozdag G, Ural D, Komsuoglu B: Magnetic Resonance Imaging Measurement of Left Ventricular Blood Flow and Coronary Flow Reserve in Patients with Chronic Heart Failure due to Coronary Artery Disease. Acta Radiol 2007:1-9.

60. Watzinger N, Lund GK, Saeed M, Reddy GP, Araoz PA, Yang M, Schwartz AB, Bedigian M, Higgins CB: Myocardial blood flow in patients with dilated cardiomyopathy: quantitative assessment with velocity-encoded cine magnetic resonance imaging of the coronary sinus. J Magn Reson Imaging 2005, 21(4):347-353.

61. van Rossum AC, Visser FC, Hofman MB, Galjee MA, Westerhof N, Valk J: Global left ventricular perfusion: noninvasive measurement with cine MR imaging and phase velocity mapping of coronary venous outflow. Radiology 1992, 182(3):685-691.

62. Kawada N, Sakuma H, Yamakado T, Takeda K, Isaka N, Nakano T, Higgins CB: Hypertrophic cardiomyopathy: MR measurement of coronary blood flow and vasodilator flow reserve in patients and healthy subjects. Radiology 1999, 211(1):129-135.

63. Pries AR, Habazettl H, Ambrosio G, Hansen PR, Kaski JC, Schachinger V, Tillmanns H, Vassalli G, Tritto I, Weis M et al: A review of methods for assessment of coronary microvascular disease in both clinical and experimental settings. Cardiovascular research 2008, 80(2):165-174.

64. Nishino M, Hoshida S, Egami Y, Kondo I, Shutta R, Yamaguchi H, Tanaka K, Tanouchi J, Hori M, Yamada Y: Coronary flow reserve by contrast enhanced transesophageal coronary sinus Doppler measurements can evaluate diabetic microvascular dysfunction. Circ J 2006, 70(11):1415-1420.

65. Schindler TH, Nitzsche EU, Munzel T, Olschewski M, Brink I, Jeserich M, Mix M, Buser PT, Pfisterer M, Solzbach U et al: Coronary vasoregulation in patients with various risk factors in response to cold pressor testing: contrasting myocardial blood flow responses to short- and long-term vitamin C administration. Journal of the American College of Cardiology 2003, 42(5):814-822.

66. Ganz W, Tamura K, Marcus HS, Donoso R, Yoshida S, Swan HJ: Measurement of coronary sinus blood flow by continuous thermodilution in man. Circulation 1971, 44(2):181-195.

67. Mundigler G, Zehetgruber M, Christ G, Siostrzonek P: Comparison of transesophageal coronary sinus and left anterior descending coronary artery Doppler measurements for the assessment of coronary flow reserve. Clinical cardiology 1997, 20(3):225-231.

68. Britten MB, Zeiher AM, Schachinger V: Microvascular dysfunction in angiographically normal or mildly diseased coronary arteries predicts adverse cardiovascular long-term outcome. Coronary artery disease 2004, 15(5):259-264.

69. Drexler H: Endothelial dysfunction: clinical implications. Progress in cardiovascular diseases 1997, 39(4):287-324.

70. Schindler TH, Nitzsche EU, Olschewski M, Brink I, Mix M, Prior J, Facta A, Inubushi M, Just H, Schelbert HR: PET-measured responses of MBF to cold pressor testing correlate with indices of coronary vasomotion on quantitative coronary angiography. J Nucl Med 2004, 45(3):419-428.

71. Olson MB, Kelsey SF, Matthews K, Shaw LJ, Sharaf BL, Pohost GM, Cornell CE, McGorray SP, Vido D, Bairey Merz CN: Symptoms, myocardial ischaemia and quality of life in women: results from the NHLBI-sponsored WISE Study. European heart journal 2003, 24(16):1506-1514.

72. Weinstein AR, Sesso HD, Lee IM, Rexrode KM, Cook NR, Manson JE, Buring JE, Gaziano JM: The joint effects of physical activity and body mass index on coronary heart disease risk in women. Archives of internal medicine 2008, 168(8):884-890.

73. Sheifer SE, Canos MR, Weinfurt KP, Arora UK, Mendelsohn FO, Gersh BJ, Weissman NJ: Sex differences in coronary artery size assessed by intravascular ultrasound. American heart journal 2000, 139(4):649-653.

74. Bansmann PM, Priest AN, Muellerleile K, Stork A, Lund GK, Kaul MG, Adam G: MRI of the coronary vessel wall at 3 T: comparison of radial and cartesian k-space sampling. Ajr 2007, 188(1):70-74.

75. Schindler TH, Hornig B, Buser PT, Olschewski M, Magosaki N, Pfisterer M, Nitzsche EU, Solzbach U, Just H: Prognostic value of abnormal vasoreactivity of epicardial coronary arteries to sympathetic stimulation in patients with normal coronary angiograms. Arteriosclerosis, thrombosis, and vascular biology 2003, 23(3):495-501.

76. Hundley WG, Lange RA, Clarke GD, Meshack BM, Payne J, Landau C, McColl R, Sayad DE, Willett DL, Willard JE et al: Assessment of coronary arterial flow and flow reserve in humans with magnetic resonance imaging. Circulation 1996, 93(8):1502-1508.

77. Sakuma H, Kawada N, Takeda K, Higgins CB: MR measurement of coronary blood flow. J Magn Reson Imaging 1999, 10(5):728-733.

78. Lund GK, Wendland MF, Shimakawa A, Arheden H, Stahlberg F, Higgins CB, Saeed M: Coronary sinus flow measurement by means of velocity-encoded cine MR imaging: validation by using flow probes in dogs. Radiology 2000, 217(2):487-493.

79. Nabel EG, Ganz P, Gordon JB, Alexander RW, Selwyn AP: Dilation of normal and constriction of atherosclerotic coronary arteries caused by the cold pressor test. Circulation 1988, 77(1):43-52.

80. Schwitter J, DeMarco T, Kneifel S, von Schulthess GK, Jorg MC, Arheden H, Ruhm S, Stumpe K, Buck A, Parmley WW et al: Magnetic resonance-based assessment of global

coronary flow and flow reserve and its relation to left ventricular functional parameters: a comparison with positron emission tomography. Circulation 2000, 101(23):2696-2702.

81. Priest AN, Bansmann PM, Mullerleile K, Adam G: Coronary vessel-wall and lumen imaging using radial k-space acquisition with MRI at 3 Tesla. European radiology 2007, 17(2):339-346.

82. Hood WB, Jr.: Regional venous drainage of the human heart. British heart journal 1968, 30(1):105-109.

83. Nitenberg A, Paycha F, Ledoux S, Sachs R, Attali JR, Valensi P: Coronary artery responses to physiological stimuli are improved by deferoxamine but not by L-arginine in non-insulin-dependent diabetic patients with angiographically normal coronary arteries and no other risk factors. Circulation 1998, 97(8):736-743.

84. Nitenberg A, Valensi P, Sachs R, Dali M, Aptecar E, Attali JR: Impairment of coronary vascular reserve and ACh-induced coronary vasodilation in diabetic patients with angiographically normal coronary arteries and normal left ventricular systolic function. Diabetes 1993, 42(7):1017-1025.

FIGURES

Figure 1. Representative SSFP cine images (short axis view, mid-ventricular slice)

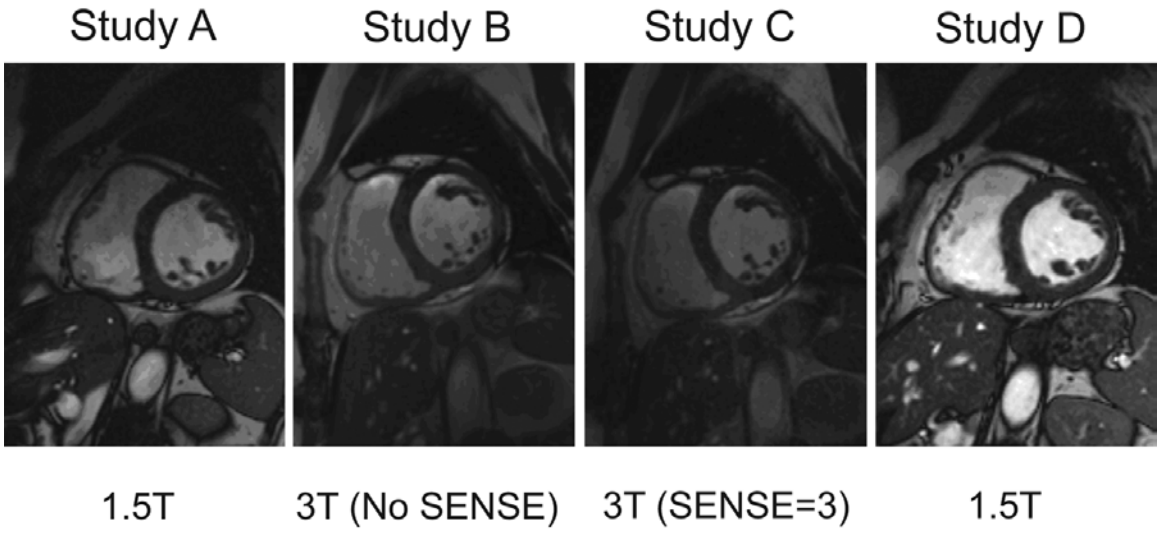

Figure 2. Coefficients of variability for cardiac structure and functional measurements

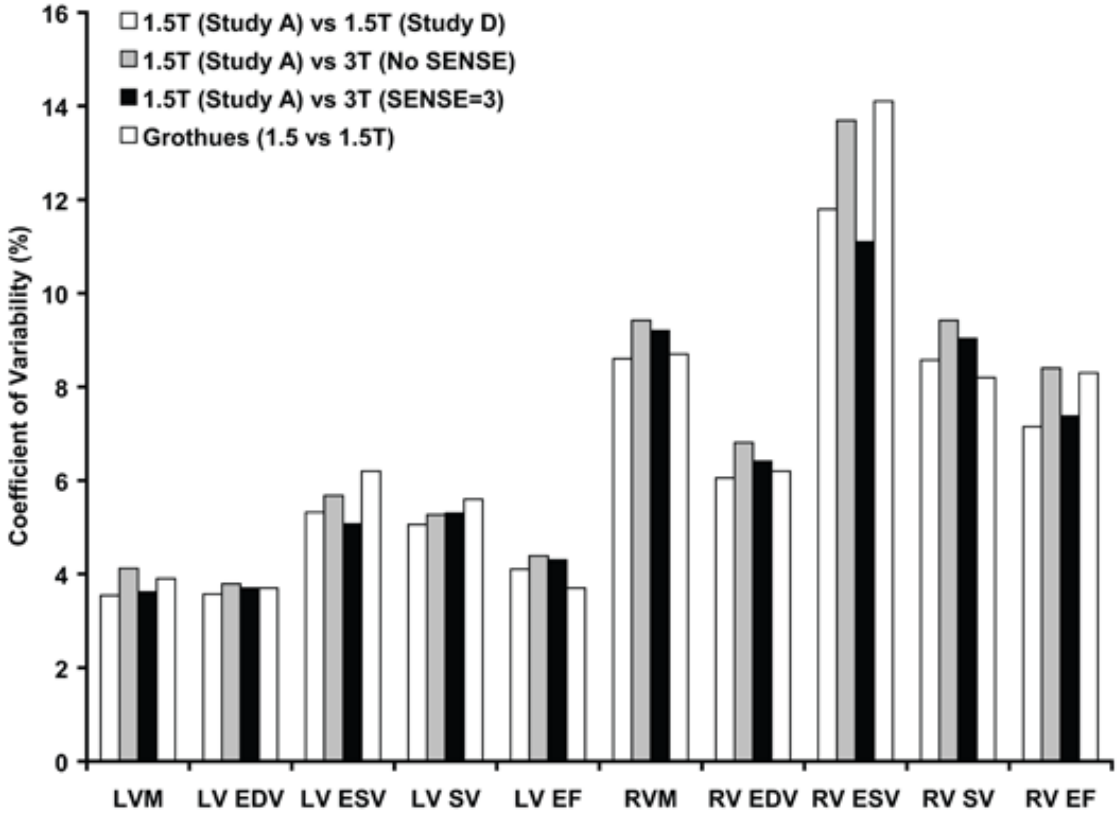

Figure 3. Bland-Altman plots comparing interstudy reproducibility between 1.5T and 3T with SENSE to the interstudy reproducibility between two 1.5T studies for **(a)** LVM, **(b)** LV EF, **(c)** RVM, and **(d)** RV EF. Limits of agreement (95%) are depicted by blue lines (1.5T vs 3T, SENSE) and pink lines (1.5T vs 1.5T).

(A)

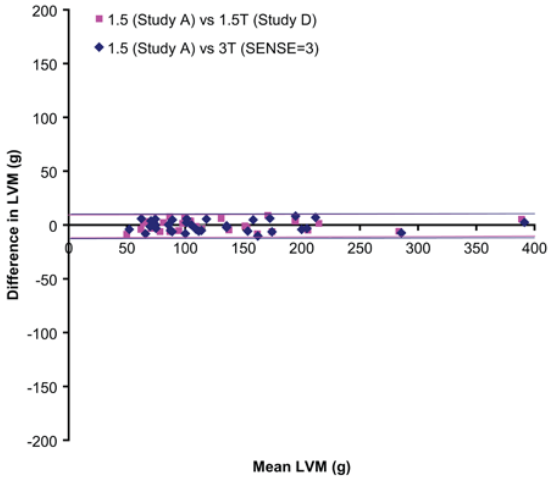

(B)

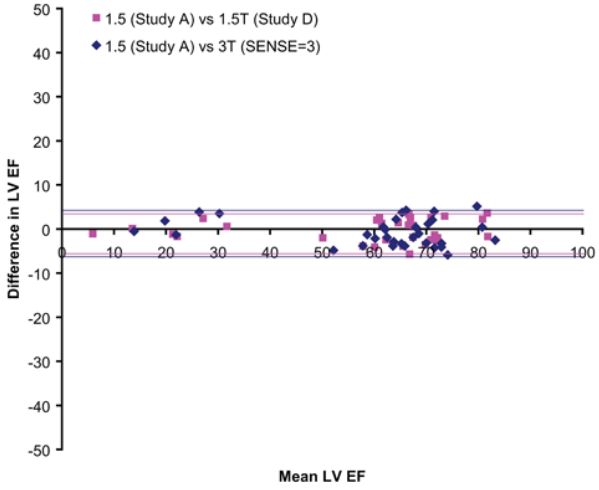

(C)

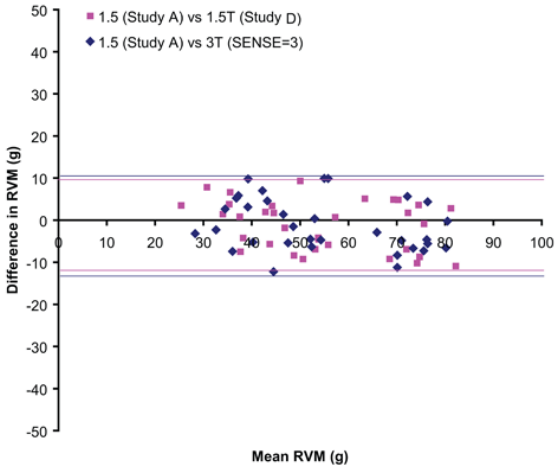

(D)

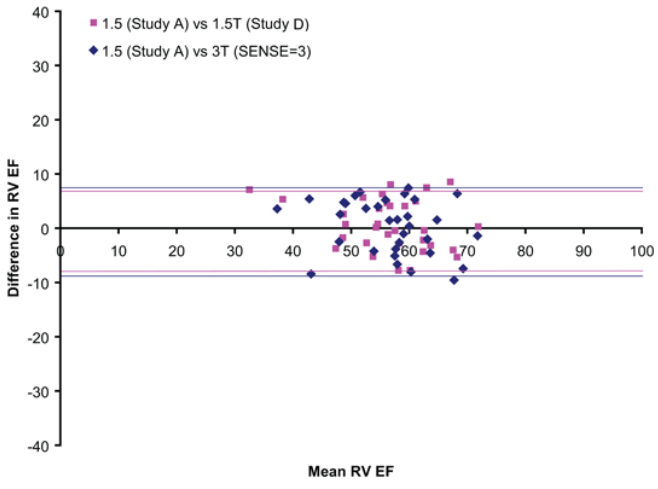

Figure 5. Representative black-blood abdominal aorta MR images.

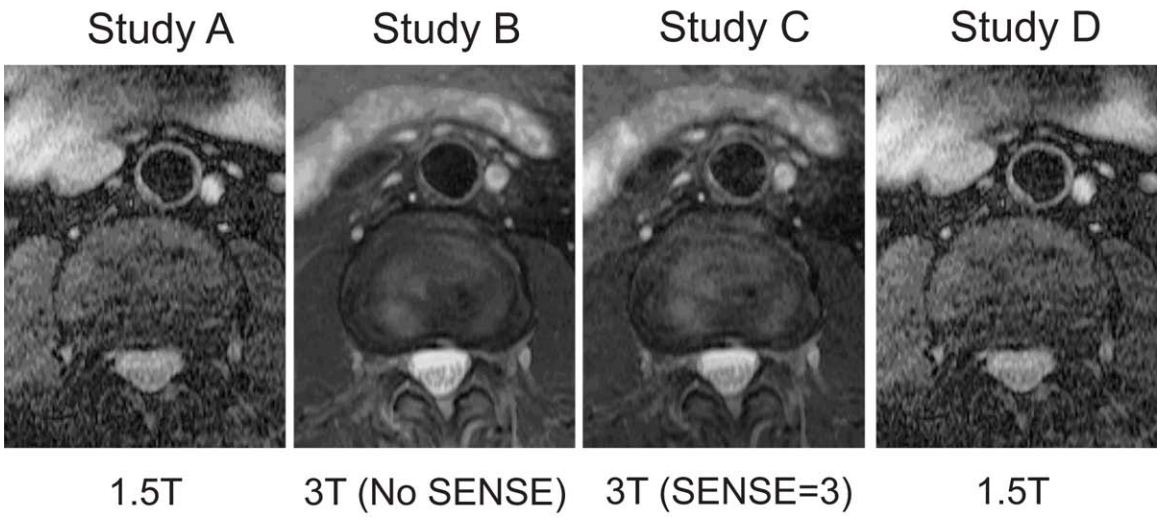

Figure 6. Coefficients of Variability for Aortic Atherosclerosis Imaging

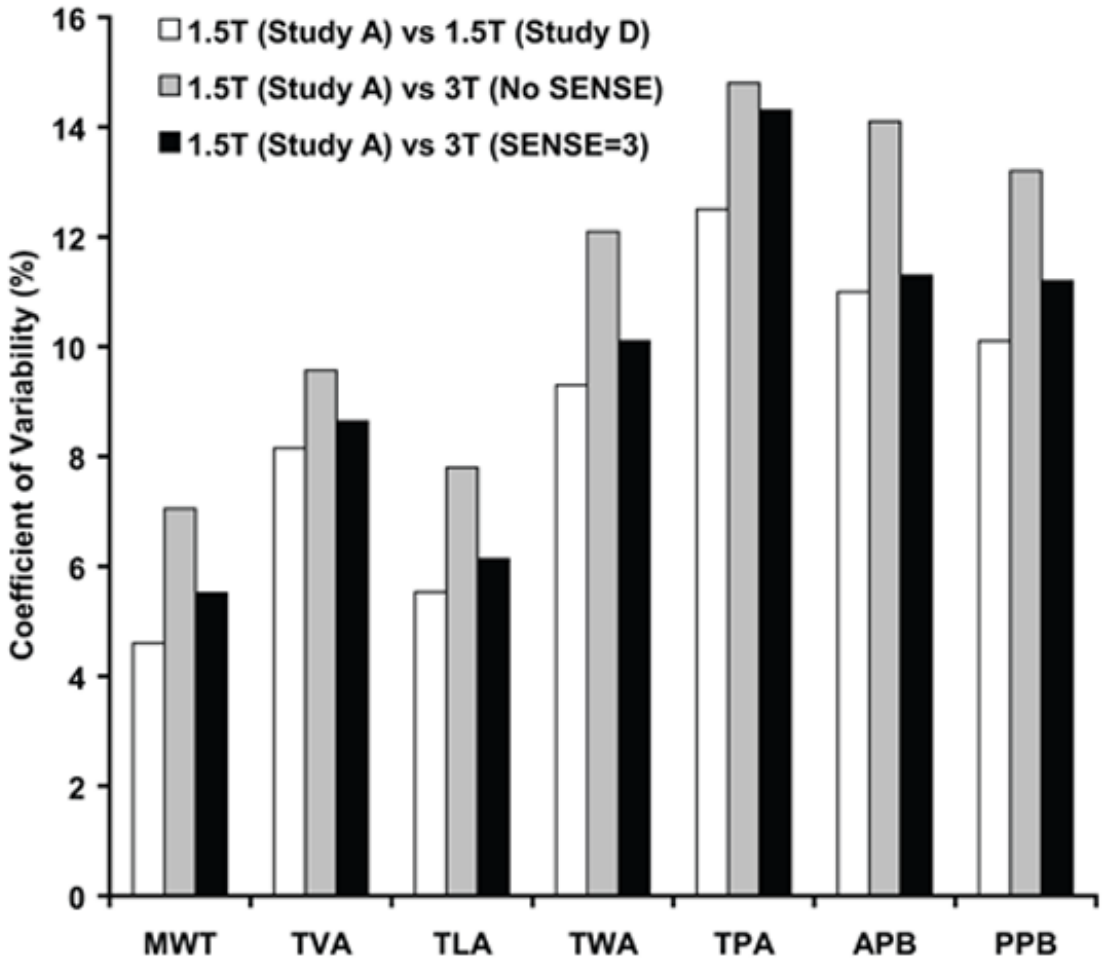

Figure 7. Bland-Altman plots describing interstudy reproducibility of **(a)** MWT and **(b)** APB obtained between 1.5-T (Study A) and 1.5-T (Study B) (■), and between 1.5-T (Study A) and 3-T (SENSE=3) (◆). Limits of agreement (95%) are depicted by pink lines (1.5-T vs 1.5-T) and blue lines (1.5-T vs 3-T, SENSE=3).

(A)

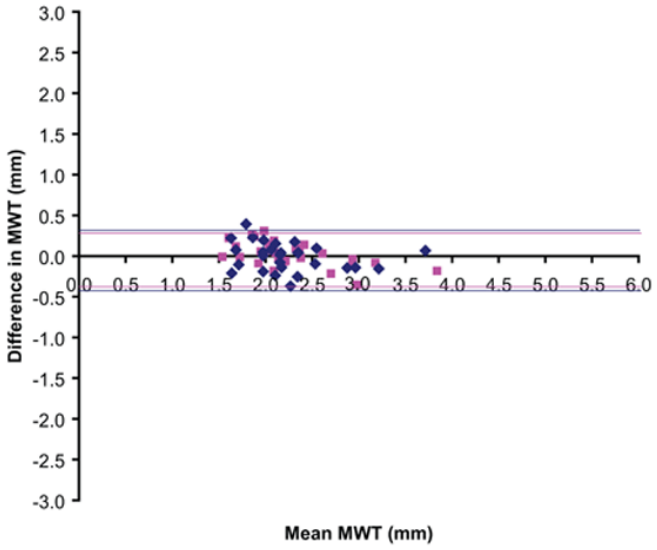

(B)

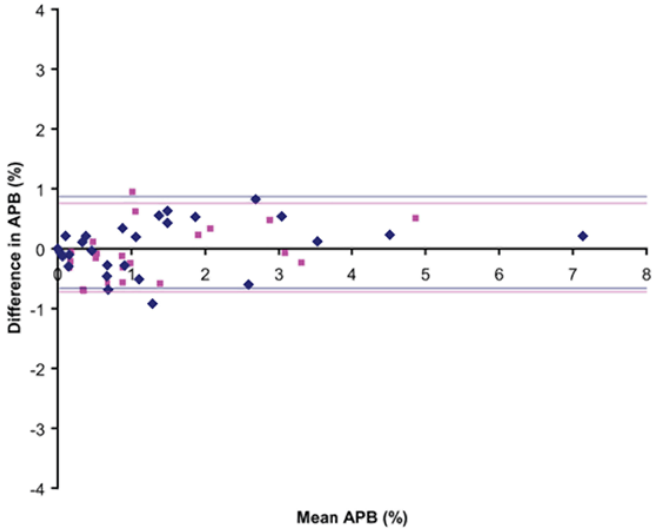

Figure 8. Coronary sinus flow imaging by VEC MRI at 3 Tesla. (A) Axial B-TFE scout image of the CS with slice orientation for flow imaging (*solid line*). Representative phase-contrast velocity-encoded images are depicted: (B) magnitude image, and (C) velocity image of the CS (*arrows*).

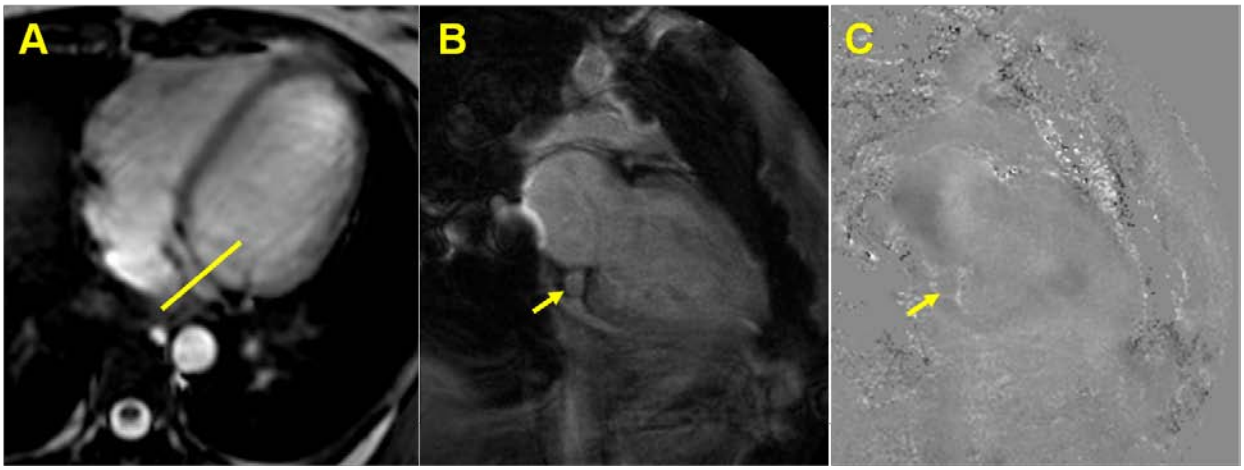

Figure 9. Representative phasic changes in coronary sinus volume flow (A), flow velocity (B), and cross-sectional area (C) throughout the cardiac cycle. Data is shown at baseline (*blue*) and at peak stress (*red*).

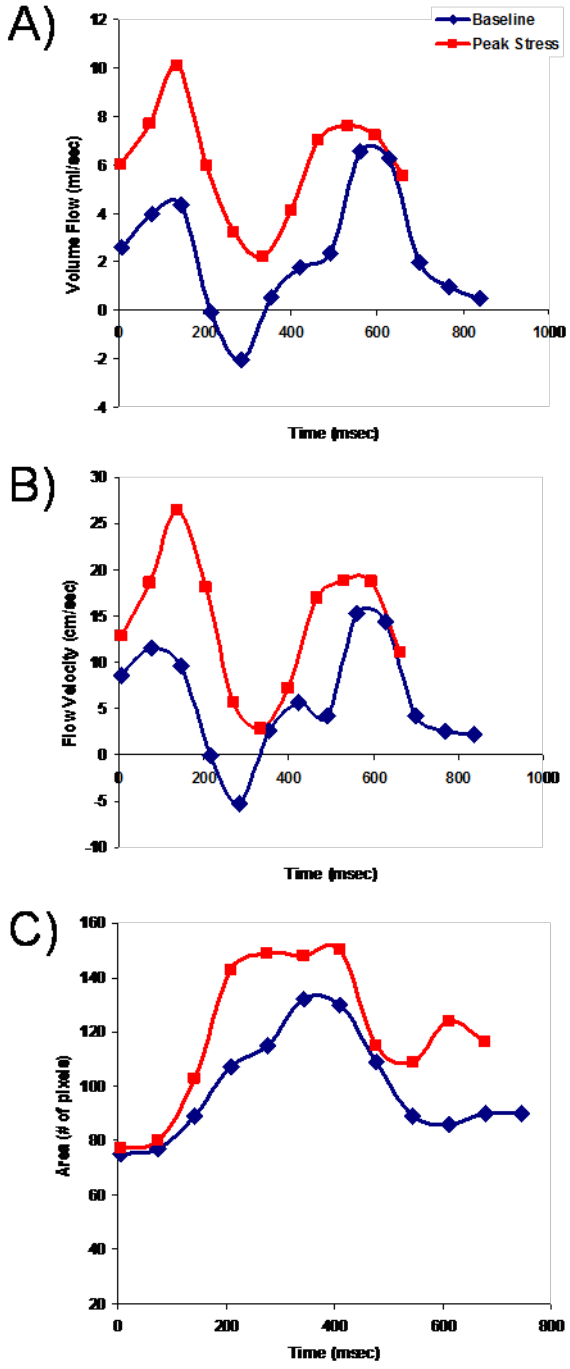

Figure 10. CS volume flow at baseline, during cold pressor stress (CPT), and during recovery. * denotes $p < 0.05$ compared to baseline. All data are expressed as sample means, with error bars representing SD.

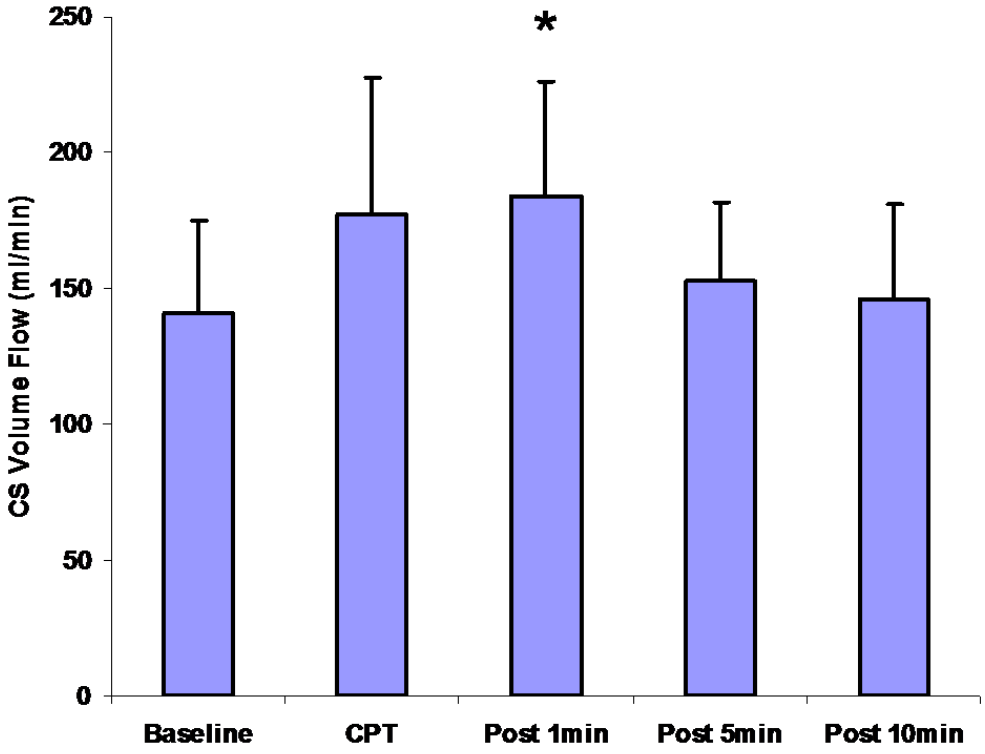

Figure 11. Correlation between CS volume flow and RCA flow velocity at baseline (*blue line*, r=0.94) and during peak cold pressor stress (*red line*, r=0.86).

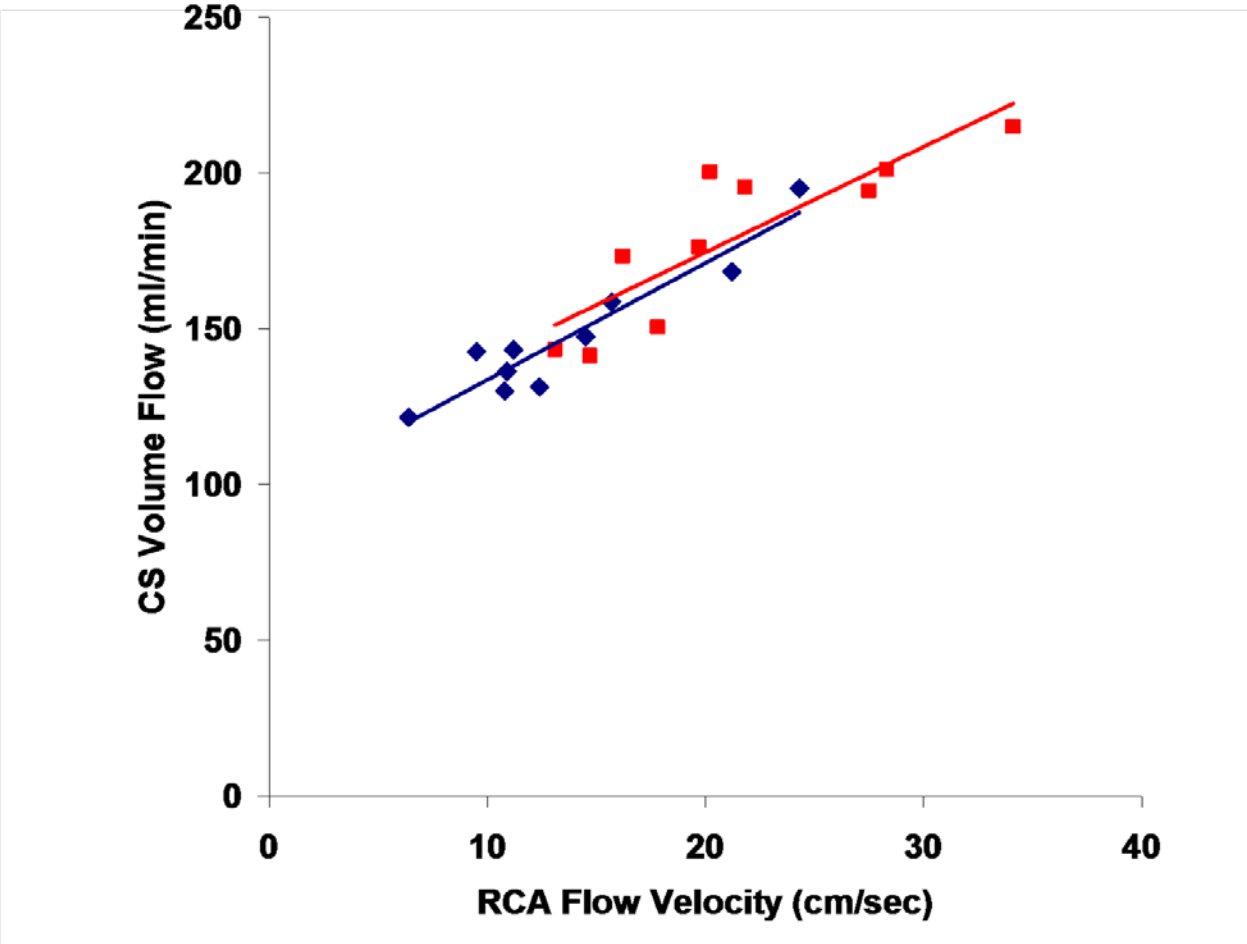

TABLES

Table 1. Characteristics of study population*

	Normal Subjects (n=20)	**Impaired LV Function (n=12)**	**Total (n=32)**
Age (yrs)	51 ± 14	52 ± 10	51 ± 12
Body mass index (kg/m^2)	24.0 ± 2.8	30.6 ± 7.9	27.2 ± 6.7
Body surface area (m^2)	1.82 ± 0.27	2.18 ± 0.16	1.96 ± 0.29
Male	8 (36%)	11 (79%)	19 (53%)
Female	14 (64%)	3 (21%)	17 (47%)
LVM (g)	97 ± 31	198 ± 93	136 ± 72
LV EDV (ml)	119 ± 32	265 ± 130	172 ± 107
LV ESV (ml)	41 ± 15	158 ± 140	87 ± 104
LV SV (ml)	80 ± 22	99 ± 20	87 ± 23
LV EF (%)	67 ± 7	43 ± 24	58 ± 18
RVM (g)	54 ± 12	67 ± 19	60 ± 17
RV EDV (ml)	130 ± 38	187 ± 51	152 ± 54
RV ESV (ml)	54 ± 20	80 ± 44	65 ± 36
RV SV (ml)	78 ± 20	86 ± 26	81 ± 26
RV EF (%)	60 ± 6	52 ± 11	57 ± 9

* Cardiac measurements are presented as population mean ± SD from the results of Study A.

LV=left ventricle; RV=right ventricle; LVM=left ventricular mass; RVM=right ventricular mass; EDV=end-diastolic volume; ESV=end-systolic volume; SV=stroke volume; EF=ejection fraction.

Table 2. Signal and contrast measurements

	1.5T (Study A)	**3T (No SENSE)**	**3T (SENSE=3)**
SNR_{Myo}	12.0 ± 3.4	24.5 ± 7.8*	14.2 ± 4.2
SNR_{LVB}	55.6 ± 8.8	108.4 ± 21.4*	62.6 ± 9.2*
SNR_{RVB}	44.5 ± 5.2	82.3 ± 13.4*	47.5 ± 7.3
CNR_{LV}	43.8 ± 6.5	83.9 ± 14.5*	48.4 ± 7.4*
CNR_{LV} Difference	n.a.	+92%	+11%
CNR_{RV}	32.9 ± 5.7	57.5 ± 12.2*	33.2 ± 6.8
CNR_{RV} Difference	n.a.	+75%	+1%

* $P < 0.05$ compared to 1.5T (Study A)

SNR=signal-to-noise ratio; CNR=contrast-to-noise ratio; Myo=septal myocardium; LV=left ventricle; RV=right ventricle; LVB=left ventricular blood pool; RVB=right ventricular blood pool

Table 3. Interstudy bias ± SD for cardiac measurements (95% limits of agreement) between methods

	1.5T (Study A) vs 1.5T (Study D)	**1.5T (Study A) vs 3T (No SENSE)**	**1.5T (Study A) vs 3T (SENSE=3)**
LVM (g)	-0.3 ± 4.9 (-10.2 to 9.5)	-0.8 ± 5.3 (-11.5 to 9.9)	-0.9 ± 5.2 (-11.4 to 9.5)
LV EDV (ml)	0.3 ± 6.3 (-12.3 to 12.9)	0.5 ± 6.4 (-12.3 to 13.4)	0.4 ± 6.3 (-12.3 to 13.1)
LV ESV (ml)	0.4 ± 4.8 (-9.2 to 9.9)	-0.2 ± 4.8 (-9.9 to 9.4)	-0.7 ± 4.5 (-9.7 to 8.3)
LV SV (ml)	0.2 ± 4.5 (-8.8 to 9.2)	0.6 ± 4.7 (-8.8 to 10.0)	0.5 ± 4.6 (-8.7 to 9.8)
LV EF	-0.4 ± 2.7 (-5.8 to 5.0)	-0.6 ± 2.9 (-6.3 to 5.1)	-0.8 ± 3.0 (-6.9 to 5.2)
RVM (g)	-1.7 ± 5.2 (-12.2 to 8.7)	-2.0 ± 5.9 (-13.9 to 9.9)	-2.2 ± 5.8 (-13.8 to 9.4)
RV EDV (ml)	-0.3 ± 8.9 (-18.3 to 17.6)	-0.4 ± 10.5* (-21.4 to 20.6)	-1.1 ± 9.6 (-20.3 to 18.1)
RV ESV (ml)	-0.5 ± 7.0 (-14.6 to 13.6)	0.4 ± 7.8 (-15.3 to 16.2)	0.3 ± 7.4 (-14.6 to 15.3)
RV SV (ml)	-0.7 ± 6.8 (-14.4 to 12.8)	-2.1 ± 7.4 (-17.0 to 12.7)	-1.9 ± 7.1 (-16.2 to 12.3)
RV EF	-0.4 ± 3.5 (-7.5 to 6.7)	-1.2 ± 5.1* (-11.4 to 9.0)	-0.9 ± 4.2 (-9.4 to 7.5)

***** $P < 0.05$ compared to the interstudy variability of two 1.5T exams

Table 4. Sample sizes required to detect changes in cardiac parameters by SSFP CMR*

	Clinically Important Change	FLASH[a]	SSFP	
		Initial: 1.5T	Initial: 1.5T	Initial: 1.5T
		Follow-up: 1.5T	Follow-up: 1.5T	Follow-up: 3T (SENSE)
LVM	10 g	13	6	8
LV EDV	10 ml	10	8	8
LV ESV	10 ml	7	5	5
LV SV	10 ml	6	4	4
LV EF	3 %	11	12	14
RVM	10 g	n.a.	7	10
RV EDV	10 ml	n.a.	17	18
RV ESV	10 ml	n.a.	10	12
RV SV	10 ml	n.a.	10	11
RV EF	5 %	n.a.	10	12

*Calculations assume power = 90% with α-error = 0.05

[a] Sample size calculations reported by Grothues et al.(4)

Table 5. Characteristics of Study Population for Aortic Atherosclerosis Imaging*

Continuous Variables, Mean ± SD	
Age (yrs)	51 ± 12
Body mass index (kg/m^2)	27.2 ± 6.7
Body surface area (m^2)	1.96 ± 0.29
Gender, No.(%)	
Male	17 (53)
Female	15 (47)
Ethnicity, No.(%)	
Black	14 (44)
White	14 (44)
Hispanic	4 (12)
Other	0 (0)
Cardiovascular Disease, No.(%)	
Composite cardiovascular disease	12 (38)
History of Myocardial Infarction	6 (19)
History of Stroke	1 (3)
History of Coronary Stenting	6 (19)
Dilated Cardiomyopathy	2 (14)
Aortic Plaque Detected, No.(%)	21 (66)
Aortic Atherosclerosis, Mean ± SD *	
TVA (mm^2)	1620 ± 318
TLA (mm^2)	1140 ± 224
TWA (mm^2)	473 ± 96
TPA (mm^2)	28 ± 33
MWT (mm)	2.26 ± 0.45
APB (%)	2.9 ± 3.1
PPB (%)	8.1 ± 11.3

* Atherosclerosis measurements were averaged from the results of Study A (1.5-T). TVA = total vascular area; TLA = total luminal area; TWA= total wall area; TPA = total plaque area; MWT = mean wall thickness; APB = area plaque burden; PPB = perimeter plaque burden.

Table 6. Image quality and contrast measurements

	1.5-T (Study A)	**3-T (No SENSE)**	**3-T (SENSE=3)**
Image Quality	4.0 ± 0.6	4.4 ± 0.5*	4.2 ± 0.7
SNR_w	11.3 ± 1.6	19.4 ± 1.9**	11.2 ± 1.7
SNR_L	1.2 ± 1.1	1.8 ± 1.2*	1.1 ± 1.0
CNR	10.1 ± 1.4	17.4 ± 2.0**	10.0 ± 1.4

* $P < 0.05$ compared to 1.5-T (Study A)

** $P < 0.001$ compared to 1.5-T (Study A)

Table 7. Interstudy Bias (mean) and Random Error (SD) for Aortic Measurements between Methods.

	1.5-T (Study A) vs 1.5-T (Study D)	**1.5-T (Study A) vs 3-T (No SENSE)**	**1.5-T (Study A) vs 3-T (SENSE=3)**
TVA (mm^2)	25 ± 132 (-239 to 289)	40 ± 155 (-270 to 350)	-11 ± 140 (-291 to 269)
TLA (mm^2)	-15 ± 63 (-141 to 111)	4 ± 89 (-174 to 182)	-21 ± 70 (-161 to 119)
TWA (mm^2)	-10 ± 44 (-98 to 78)	-8 ± 57 (-122 to 106)	-15 ± 48 (-111 to 81)
MWT (mm)	-0.03 ± 0.09 (-0.21 to 0.15)	0.01 ± 0.17 (-0.33 to 0.35)	-0.01 ± 0.12 (-0.27 to 0.25)
TPA (mm^2)	-0.8 ± 3.5 (-7.8 to 6.2)	-2.4 ± 4.4 (-11.2 to 6.4)	-0.4 ± 4.0 (-8.4 to 7.6)
APB (%)	-0.02 ± 0.32 (-0.66 to 0.62)	0.06 ± 0.41 (-0.76 to 0.87)	0.11 ± 0.33 (-0.55 to 0.77)
PPB (%)	-0.10 ± 0.82 (-1.74 to 1.54)	-0.09 ± 1.07 (-2.23 to 2.05)	-0.05 ± 0.91 (-1.87 to 1.77)

Note: Limits of agreement (95%) are shown in parentheses.

* $P < 0.05$ vs. interstudy reproducibility between 1.5-T (Study A) and 1.5-T (Study D)

Table 8. Sample Sizes Required to Detect Clinical Changes in Aortic Measurements

	Clinically Significant Change**	**Sample size requirements***		
		Follow-Up: 1.5-T	**Follow-Up: 3-T (No SENSE)**	**Follow-Up: 3-T (SENSE=3)**
TVA	150 mm^2	16	22	18
TLA	75 mm^2	15	30	18
TWA	50 mm^2	16	27	19
TPA	10 mm^2	5	8	5
MWT	0.25 mm	8	16	10
APB	0.5 %	9	13	9
PPB	1 %	14	24	17

Note: Sample size calculations assume 90% power with α-error of 0.05.

*All values are based upon an initial 1.5-T imaging study with variable follow-up imaging modalities

** Values approximate significant changes reported by Corti et al.(53)

Table 9. Characteristics of the Study Group for Coronary Sinus Flow Imaging (n=10)

Age (years, mean ± SD)	38 ± 10
Body mass index (kg/m^2, mean ± SD)	33 ± 8
Ethnic background	
Caucasian (%)	40
Black (%)	30
Hispanic (%)	20
Asian (%)	10
Cardiovascular Risk Factors	
Diabetes Mellitus (%)	60
Hyperlipidemia (%)	20
Previous history of smoking (%)	10
Obesity* (%)	50
Family history of coronary artery disease (%)	20

*Obesity is defined as a body mass index > 30 kg/m^2

Table 10. Change in hemodynamics and CS flow measurements after cold pressor stress*

Measurement	Baseline (Rest)	Peak Stress	% Change	**P value
CS volume flow (ml/min)	141 ± 34	184 ± 42	24 ± 6	0.02
CS flow velocity (cm/sec)	11.0 ± 4.0	16.3 ± 5.7	38 ± 16	0.02
CS area (mm^2)	76.5 ± 19	84.8 ± 18	12 ± 7	0.11
RCA flow velocity (cm/sec)	15.3 ± 5	23.2 ± 7	56 ± 37	< 0.01
Rate-pressure product (mmHg/min)	6947 ± 954	10,033 ± 2039	45 ± 26	< 0.01
Diastolic BP (mmHg)	69 ± 7	80 ± 9	16 ± 12	< 0.01

* Data are expressed as mean ± SD

** Comparing baseline to peak stress by paired t-test

ACKNOWLEDGEMENTS

I would like to thank the following faculty and staff members for their fantastic support and guidance throughout my research projects:

Dr. Ronald M. Peshock

Dr. Roderick McColl

Dr. Amit Khera

Dr. Alice Chang

Dr. Ivan Dimitrov

Dr. Melonie Kotys

Dr. Milton Packer

Dr. Paul Weatherall

Dr. Robert Parkey

Dr. Michael McPhaul

Dr. Andrew Kontak

Tommy Tillery

Victoria Vescovo

Colby Ayers

VITAE

Christopher Maroules was born in Anchorage, Alaska in 1981. His family relocated to San Diego when he was two years old, and it was there that Christopher developed a love for the ocean and the outdoors. At the age of seven, Christopher's father accepted a faculty position at Illinois State University in Bloomington, Illinois, and his family relocated once again. The greater part of Christopher's adolescence and young adult life was spent in Central Illinois. Christopher and his twin brother, Nick, attended Bloomington High School where Christopher played varsity football and tennis and graduated Class Valedictorian. During high school, Christopher first developed a strong interest in science and medicine. After being awarded a Presidential Scholarship at Illinois State University, Christopher decided he would remain local for his college education and pursue a bachelor's degree in Biochemistry.

College was an exciting time in Christopher's personal and professional life. His academic interests in medical imaging originated from his experience working in an organic chemistry laboratory at Illinois State. It was there he became introduced to nuclear magnetic resonance (NMR) spectroscopy and quickly discovered its analytical capabilities for elucidating molecular structure. In the summer of 2002, Christopher was awarded a NIH Biomedical Research Fellowship and spent several months investigating coagulation physiology using proton NMR. Working at the NIH was exciting for Christopher because it offered him insight into patient-oriented research while affording the opportunity to interact with many wonderful physician-scientists. In addition, the NIH first exposed Christopher to clinical MRI after his mentor suggested that he participate in an investigational imaging study at Warren Magnuson Clinical Center. During his free time in college, Christopher volunteered at the Community

Cancer Center and enjoyed cross training and weightlifting. During his senior year, Christopher comitted himself to a career in medicine and was accepted at the Indiana University School of Medicine. He graduated from Illinois State summa cum laude in Spring 2003, and was one of eight recipients of the Robert G. Bone Scholarship.

Christopher's preclinical years at Indiana University School of Medicine were both challenging and rewarding. Although he dedicated numerous hours towards learning the pathophysiology of disease and the fundamentals of patient care, he had ample time to participate in many of his favorite outdoor activities such as camping, hiking, and tennis. By the end of his second year of medical school, Christopher's long hours in the classroom had made him nostalgic for research. So, in the Spring of 2006 Christopher applied for a Doris Duke Clinical Research Fellowship and was awarded one at the University of Texas Southwestern Medical Center in Dallas.

Accepting a Doris Duke Fellowship in Dallas was a wise decision for Christopher, both professionally and personally. Throughout the fellowship year he worked closely with Dr. Ronald Peshock, a pioneer and leading expert in cardiovascular MRI. Working alongside Dr. Peshock, Christopher developed accelerated MR imaging sequences for evaluating cardiac function and vascular disease at high field strength. His work helped establish the cardiac MRI protocol utilized in Phase Two of the Dallas Heart Study, one of the largest prospective cardiovascular research studies to date. Furthermore, Christopher helped design MRI protocols for measuring coronary arterial flow, and participated in a multicenter trial investigating the utility of cardiac MRI in determining risk for sudden cardiac death. However, the most rewarding aspect of Christopher's move to Dallas was that he met and fell in love with his fiancée, Allison, whom he plans to wed this coming May.

Christopher decided to make a permanent transfer to UT Southwestern Medical School in Spring 2007. Despite his demanding clinical rotation schedule, he was excited to become active in patient care once again. Christopher continued to work with Dr. Peshock during his third and forth years of medical school, although his primary focus was developing the best clinical training possible. Christopher and his fiancée moved into a home in the Summer of 2007, and have enjoyed hosting friends, traveling, and working out. Last spring, Christopher was inducted into the Alpha Omega Alpha Honorary Society at UT Southwestern. Next year he will complete a preliminary internal medicine internship at the Naval Medical Center in Virginia, followed by a residency in Diagnostic Radiology. Christopher aspires to become an academic radiologist with fellowship training in advanced cardiothoracic imaging.